BIOCHEMISTRY
including biophysical chemistry & molecular biology

Article

pubs.acs.org/biochemistry

Interaction of the Histone mRNA Hairpin with Stem–Loop Binding Protein (SLBP) and Regulation of the SLBP–RNA Complex by Phosphorylation and Proline Isomerization

Minyou Zhang,[†,‡] TuKiet T. Lam,[§] Marco Tonelli,[∥] William F. Marzluff,[⊥] and Roopa Thapar*[,†,‡]

[†]Hauptman-Woodward Medical Research Institute, 700 Ellicott Street, Buffalo, New York 14203, United States

[‡]Department of Structural Biology, SUNY at Buffalo, 700 Ellicott Street, Buffalo, New York 14203, United States

[§]W. M. Keck Foundation Biotechnology Resource Laboratory, Yale University, New Haven, Connecticut 06511, United States

[∥]National Magnetic Resonance Facility at Madison, University of Wisconsin—Madison, Madison, Wisconsin 53706, United States

[⊥]Department of Biochemistry and Biophysics, University of North Carolina at Chapel Hill, Chapel Hill, North Carolina 27599, United States

Supporting Information

ABSTRACT: In metazoans, the majority of histone proteins are generated from replication-dependent histone mRNAs. These mRNAs are unique in that they are not polyadenylated but have a stem–loop structure in their 3′ untranslated region. An early event in 3′ end formation of histone mRNAs is the binding of stem–loop binding protein (SLBP) to the stem–loop structure. Here we provide insight into the mechanism by which SLBP contacts the histone mRNA. There are two binding sites in the SLBP RNA binding domain for the histone mRNA hairpin. The first binding site (Glu129–Val158) consists of a helix–turn–helix motif that likely recognizes the unpaired uridines in the loop of the histone hairpin and, upon binding, destabilizes the first G-C base pair at the base of the stem. The second binding site lies between residues Arg180 and Pro200, which appears to recognize the second G-C base pair from the base of the stem and possibly regions flanking the stem–loop structure. We show that the SLBP–histone mRNA complex is regulated by threonine phosphorylation and proline isomerization in a conserved TPNK sequence that lies between the two binding sites. Threonine phosphorylation increases the affinity of SLBP for histone mRNA by slowing the off rate for complex dissociation, whereas the adjacent proline acts as a critical hinge that may orient the second binding site for formation of a stable SLBP–histone mRNA complex. The nuclear magnetic resonance and kinetic studies presented here provide a framework for understanding how SLBP recognizes histone mRNA and highlight possible structural roles of phosphorylation and proline isomerization in RNA binding proteins in remodeling ribonucleoprotein complexes.

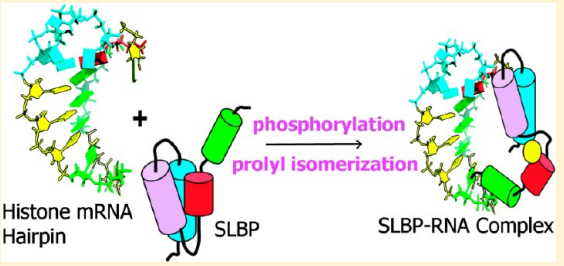

Replication-dependent histone genes encode the bulk of histone proteins in metazoans.[1] Histone proteins are important for packaging DNA into chromatin as well as for regulating gene expression via the histone code.[2,3] The mRNAs that encode for all five core histone proteins (H1, H2A, H2B, H3, and H4) are unique in that they are the only naturally occurring eukaryotic mRNAs that are not polyadenylated. Instead of a poly(A) tail, the histone pre-mRNA 3′ untranslated region (3′UTR) contains a conserved 16-nucleotide stem–loop structure (Figure 1A1) and a purine-rich sequence [termed the histone downstream element (HDE)] located 12–19 nucleotides downstream of the cleavage site (Figures 1A2 and 2B). These are the major cis elements that are required for histone pre-mRNA processing.[4,5] The highly conserved tetraloop hairpin[6,7] in the 3′UTR also includes a conserved five-nucleotide AC-rich sequence before the stem–loop structure, a 16-nucleotide stem–loop structure with a six-base stem and a four-base loop, and an AC-rich sequence of either four (in *Drosophila* and sea urchins) or five nucleotides (in vertebrates) after the stem–loop structure (Figure 1A1). This region is the binding site for stem–loop binding protein (SLBP)[8] or hairpin-binding protein (HBP)[9] (Figure 2A), and the histone mRNA–SLBP complex functions as the major regulatory element for coordinate regulation of histone mRNAs for all five histone proteins. In mammals, a number of proteins such as ZFP100,[10] FLASH,[11] symplekin,[12] components of the CPSF complex,[12,13] and possibly the U2 snRNP[14] assemble at or near the histone 3′UTR and are involved in histone pre-mRNA processing. The molecular details of these protein–nucleic acid interactions, the mode of assembly, and the dynamic rearrangements that likely occur in the ribonucleoprotein complex to catalyze endonucleolytic cleavage during 3′ end formation remain unknown.

Received: May 4, 2011
Revised: February 29, 2012
Published: March 22, 2012

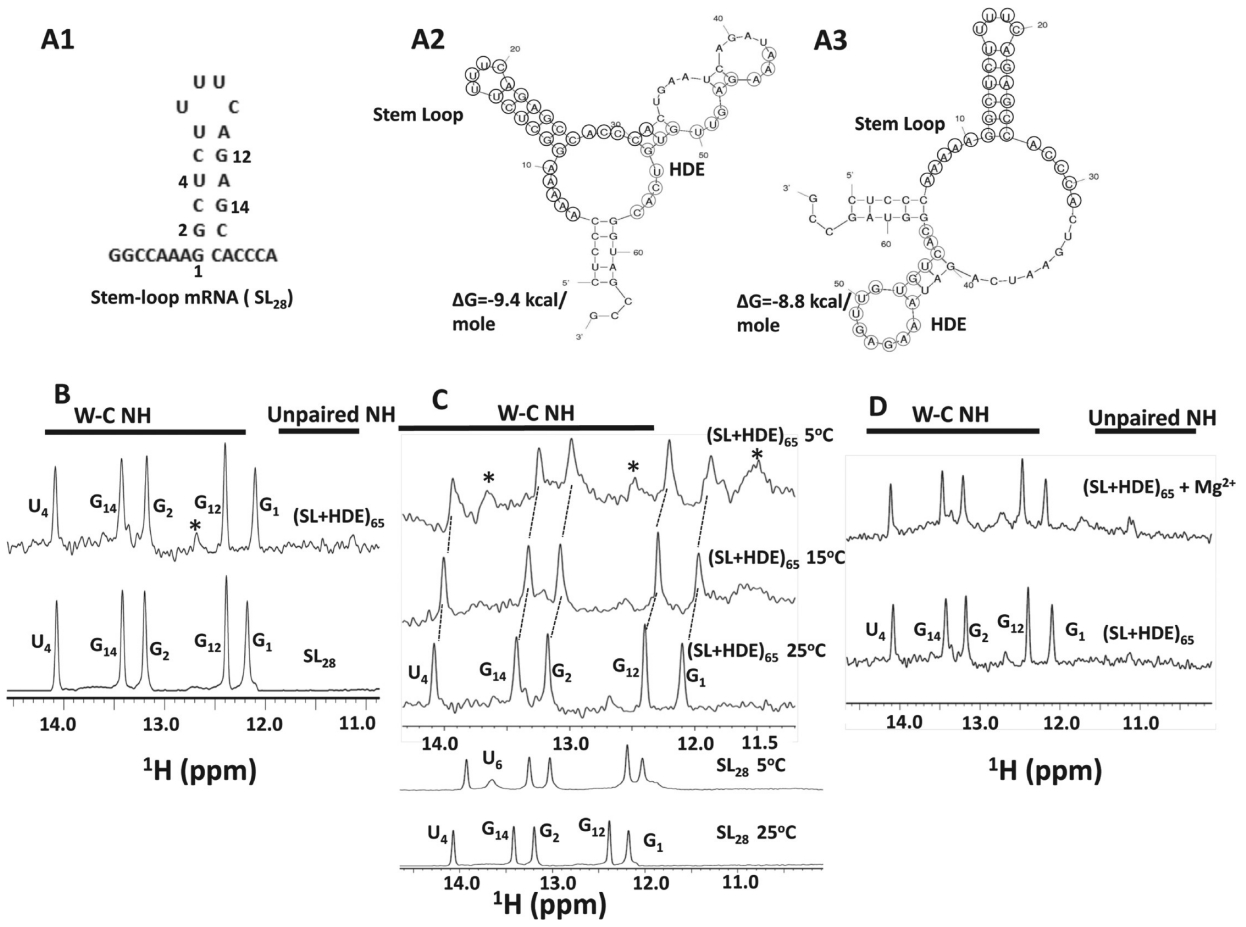

Figure 1. Structural determinants in the histone 3′UTR of the mouse H2A-614 RNA. (A1−A3) Secondary structure of the histone stem−loop (SL28) mRNA, the structure of which has previously been confirmed by nuclear magnetic resonance (NMR) (A1), and secondary structure predictions (A2 and A3) of the 65-mer (SL + HDE) corresponding to the histone 3′UTR of the mouse H2A-614 histone gene by UNAFold. The sequence corresponding to the stem−loop structure and the HDE have been highlighted in circles. (B) Comparison of one-dimensional imino proton NMR spectra of 28-nucleotide stem−loop SL28 (shown in panel A1) and the 65-mer (SL + HDE) sequence collected at 600 MHz, pH 6.8, and 25 °C. (C) Comparison of one-dimensional imino proton NMR spectra of SL28 and SL + HDE recorded at different temperatures, 600 MHz, and pH 6.8. (D) Comparison of one-dimensional imino proton NMR spectra of SL + HDE in the presence of Mg^{2+}. Assignments are given for the bottom spectra, and the numbering corresponds to that shown for the stem−loop sequence in panel A1. Asterisks show new resonances.

SLBP is important for histone pre-mRNA processing,[15] export,[16] and translation of histone mRNA.[17] The role of SLBP in histone mRNA processing has been proposed to be to stabilize the multiprotein complex with the U7 snRNP.[15] SLBP has a small, highly basic RNA binding and processing domain (RPD) that bears no sequence similarity to any other RNA binding domain (RBD) in eukaryotic genomes and is expected to have a novel fold. The SLBP RBD is a subdomain of the RPD (Figure 2A) as there are sequences in the RPD that are important for RNA processing but not RNA binding.[18] The SLBP−histone mRNA complex functions as a coordinate unit. SLBP forms a stable complex with the 26-nucleotide binding site that includes the 16-nucleotide hairpin and the conserved single-stranded 5′ and 3′ regions at the end of histone mRNAs in vivo and in vitro.[19,20] Our previous biophysical studies have shown that SLBP is an unstable protein with large segments of instrinsic disorder in the N-terminal domain,[21] and the SLBP RPD has α-helical secondary structure but not does not adopt a well-ordered tertiary structure in the absence of RNA.[19] The instrinsic disorder and instability of the SLBP RPD have made determination of the structure of the SLBP−RNA complex particularly challenging by both nuclear magnetic resonance (NMR) spectroscopy and X-ray diffraction. Previous top-down and bottom-up mass spectrometric analysis of the human and *Drosophila* SLBPs revealed that the protein is phosphorylated at an invariant threonine (in an HPKTPNK sequence) within its RNA binding domain.[22] Phosphorylation increases the affinity of SLBP for the RNA substrate by approximately 8-fold in vitro. Phosphorylation of this threonine is also essential for the viability of *Drosophila* embryos[23] and for histone pre-mRNA processing in vivo.[23] Furthermore, mutation of the proline that flanks the phosphorylated Thr to a Ser in *Caenorhabditis elegans* SLBP results in a loss of RNA binding and embryonic lethality.[24]

In this paper, we describe the structural determinants of the pre-mRNA and SLBP for sequence specific recognition of histone mRNA. We use NMR spectroscopy to show that in the absence of bound proteins and U7 snRNA, the pre-mRNA has residual secondary structure that extends beyond the stem−loop motif. However, the only stable element of secondary structure in the 3′UTR of the pre-mRNA is the 16-nucleotide hairpin. Kinetic measurements using surface plasmon resonance (SPR) show that the pre-mRNA interacts with SLBP with a 10-fold higher affinity compared to the isolated stem−loop structure. Therefore, the residual structure in the pre-mRNA may be important for interaction with SLBP and for assembly of the histone processing complex. Using baculovirus-expressed SLBPs

dx.doi.org/10.1021/bi2018255 | *Biochemistry* 2012, 51, 3215−3231

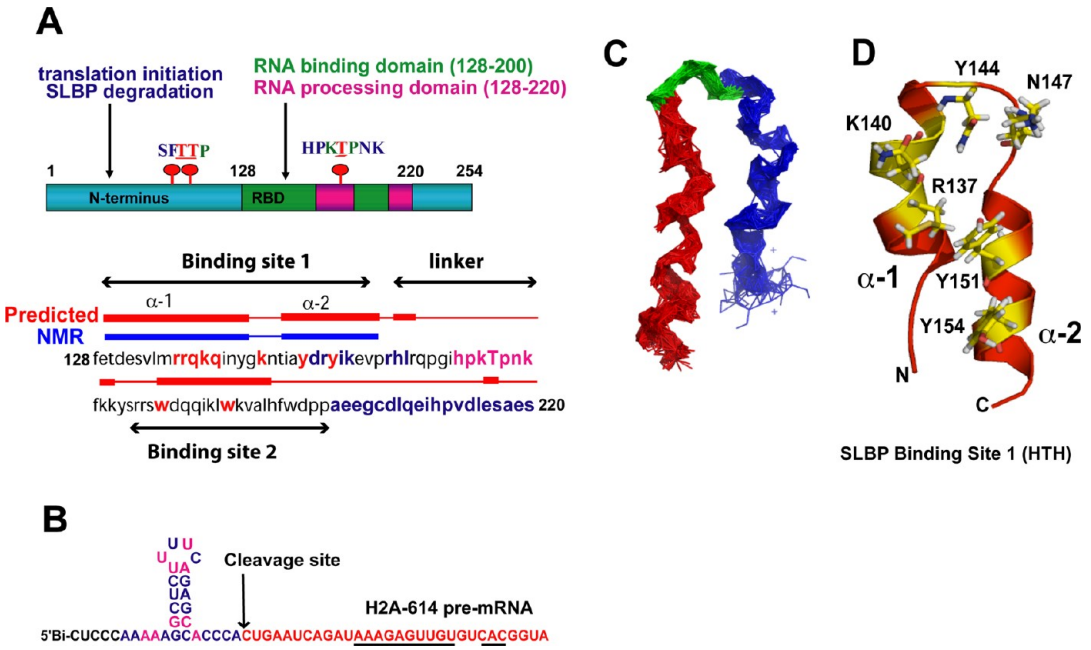

Figure 2. Solution NMR Structure of the 30-residue peptide fragment of the SLBP RNA binding and processing domain (RPD). (A) The domain structure of human SLBP consists of an N-terminal domain important for translation initiation and SLBP degradation and a central domain that has the sequence determinants for RNA binding and processing. Residues previously shown to be important for RNA binding are colored green, and residues shown to be important for RNA processing but not RNA binding are colored pink. The phosphorylated threonine in the HPKTPNK sequence is depicted. The two binding sites and the linker regions are shown. (B) Sequences of two cis elements shown to be important for histone pre-mRNA processing in the H2A-614 3′ UTR. The 26-nucleotide hairpin is conserved in all metazoans and binds SLBP. Nucleotides that are important for SLBP interaction are colored pink. The HDE sequence that base pairs with the U7 snRNP is underlined. (C) Superposition of the top 20 NMR conformers (of 100 calculated). (D) Ribbon representation of the average solution structure of the first 30 residues of the hSLBP RPD. Residues shown to be important for RNA binding from previous mutagenesis studies are depicted as sticks.

that were either fully phosphorylated or intentionally dephosphorylated at the conserved threonine in the TPNK sequence of the RNA binding domain, we show that phosphorylation of SLBP is important for the kinetics of association with the histone mRNA hairpin. The first 30 residues of the SLBP RPD have a number of arginines and tyrosines that are important determinants for sequence specific histone mRNA recognition.[18] We show that this region forms a helix−turn−helix (HTH) motif in solution that, by itself, has weak affinity for the histone mRNA stem−loop structure. NMR chemical shift mapping experiments and NOESY data for the HTH−RNA complex indicate that the HTH motif likely binds near the unpaired uridines of the loop, possibly via stacking interactions with conserved tyrosines in the SLBP HTH motif, and this interaction may destabilize the first G-C base pair at the base of the stem. ^{31}P NMR spectra of the intact phosphorylated hSLBP RPD as well as two-dimensional (2D) ^{1}H−^{1}H NOESY NMR spectra of SLBP peptides showed that the SLBP RPD interconverts between multiple conformations under physiological conditions that we attribute to proline isomerization. To provide unequivocal evidence that cis−trans proline isomerization about the Thr171/230−Pro172/231 bond is important for the instability of the SLBP RPD, we mutated Pro231 in the *Drosophila* SLBP (dSLBP) RPD to a glycine. The P231G dSLBP RPD showed a single conformer in solution and formed a stoichiometric complex with histone stem−loop RNA.

Our studies provide the first molecular insight into the mode of histone mRNA recognition by SLBP. The structural, kinetic, and functional ramifications of phosphorylation and proline isomerization of the SLBP RPD in facilitating histone mRNA recognition and processing are discussed.

MATERIALS AND METHODS

Preparation of Proteins, Peptides, and RNA. Phosphorylated human and *Drosophila* SLBPs were expressed in baculovirus as previously described.[25] The proteins used in this study were full-length *Drosophila* SLBP (dSLBP), the full-length dSLBP T230A mutant, the dSLBP RBD (residues 189−259), the dSLBP RPD (residues 189−276), and the human SLBP RPD (residues 121−219). These SLBPs were subcloned into the *Nco*I and *Xho*I restriction sites of baculovirus vector pFastBac HTA (Invitrogen) and were expressed using the Bac-to-Bac expression system (Invitrogen). All proteins have an N-terminal tag corresponding to the sequence MSYYHHHHHHDYDIPTTENLYFQGAMA. After synthesis, the methionine is removed and the α-amino group on the N-terminal serine acetylated.[22] Sf21 cells were transfected with baculovirus (at a density of 1×10^6 cells/mL) in serum-free SF900 medium (Gibco or Hyclone) and purified using nickel affinity chromatography. The identity of all proteins was confirmed by mass spectrometry. These dSLBPs gave a measured mass that corresponded to the removal of the N-terminal Met (−131), the acetylation of the Ser (+42), and the phosphorylation of Thr230 (+80) as previously described,[22] and the human protein gave similar results with T171 phosphorylated. For ^{31}P NMR studies, a 128-residue pseudo-wild-type human SLBP (hSLBP) RPD construct was designed (residues 121−219) to ensure a singly phosphorylated species at Thr171. The expressed protein consists of the following sequence: *MSYYHHHHHHDYDIPTTENLYFQGA*<u>ME</u>E<u>A</u>M<u>AA</u>VPADFETDESVLMRRQKQINYGKNTIAYDRYIKEVPRHLRQPGIHPK-(**phospho**)TPNKFKKYSRRSWDQQIKLWKVALHFWDPPAEEGCDLQEIHPVDLE<u>A</u>AE.

dx.doi.org/10.1021/bi2018255 | *Biochemistry* 2012, 51, 3215−3231

There are several non-native amino acids in this sequence. The first 25 residues at the N-terminus correspond to the vector sequence from pFastBac HTA. The N-terminal $(His)_6$ tag does not contribute to RNA binding in *Drosophila* and human SLBPs and was retained for ^{31}P NMR experiments. Several serine residues in the RPD (underlined) were mutated to alanines (and S122 was mutated to E122 to facilitate cloning). The minimal 73-amino acid RBD sequence (FET....DPP) that has been shown to be necessary and sufficient for RNA binding[18,20] was all-native. In addition, 19 amino acids of hSLBP were included at the C-terminus. These residues are important for pre-mRNA processing[25] as well as for the stability of the RBD during protein expression (R. Thapar, unpublished observations). The samples were concentrated and buffer exchanged using a G25 column in NMR buffer (GE). Where indicated, we dephosphorylated baculovirus-expressed SLBPs by treating the protein with calf intestinal phosphatase (CIP) at a molar ratio of 1:100 (SLBP:CIP) at 37 °C for 12 h. Complete dephosphorylation was determined by mobility shift for the full-length SLBP via sodium dodecyl sulfate−polyacrylamide gel electrophoresis (SDS−PAGE), in electrophoretic mobility shift assays (EMSAs), and by mass spectrometry. The dSLBP RPD P231G (residues 173−276) mutant was generated using Quickchange mutagenesis (Stratagene) and was expressed from vector pET15b. The mutant was labeled uniformly with ^{15}N by growing *Escherichia coli* in M9 minimal medium with $^{15}NH_4Cl$ as the sole source of nitrogen. The dSLBP WT and P231G RPD recombinant proteins were expressed with an N-terminal His tag and purified using nickel affinity and gel filtration chromatographies. Protein concentrations for full-length and SLBP RPD samples were measured using extinction coefficients at 280 nm of 42060 and 28420 M^{-1} cm^{-1}, respectively. Threonine-phosphorylated and unphosphorylated peptides corresponding to residues His161−Arg180 [^{161}HLRQPGIHPKTPNKFKKYSR^{180} ($WT_{20\text{-mer}}$) and ^{161}HLRQPGI**A**PKTPNKFKKYSR^{180} ($H168A_{20\text{-mer}}$), respectively] of human SLBP and a 30-residue peptide corresponding to residues Glu129−Val158 of human SLBP were synthesized by either Sigma-Genosys or Genscript. A 30-mer mutant peptide in which Y151 and Y154 were replaced with alanines and R137 and R138 were changed to lysines ($MUT_{30\text{-mer}}$) (^{129}ETDESVLM**KK**QKQINYGKNTIA**A**DR**A**IKEV^{158}) was synthesized as a control to determine the specificity of the chemical shift titrations. All peptides were at least 90% pure as determined by reverse phase high-performance liquid chromatography and matrix-assisted laser desorption ionization mass spectometry. No tags were associated with the peptides.

The following RNAs were used in this study: SL_{28}-UA (5′ GGCCAAAGGCUCUUUUCAGAGCCACCCA 3′), SL_{28}-CG (5′ GGCCAAAGGCCCUUUUCAGGGCCACCCA 3′), LSL_{28}-CG (5′ GGCCAAAGGCCCUAUACAGGGCCACCCA 3′), RSL28-CG (5′ GGCCAAACCGGGUUUUCACCCGGACCCA 3′), and the 65-nucleotide pre-mRNA (5′ CUCCCAAAAAGGCUCUUUUCAGAGCCACCCACUGAAUCAGAUAAAGAGUUGUGUCACGGUAGCCC 3′). Two different SL_{28} RNAs with either a UA or a CG base pair at position 4 of the stem were used as noted in the figure legends. In mammals, the residue at position 4 is variable in that all H4 histone mRNAs have a CG at this position whereas all other histone mRNAs have a UA. Replacing a CG with UA has no effect on SLBP binding.[20] The LSL_{28}-CG mutant has two unpaired uridines in the loop (U7 and U9) mutated to adenosines. Stem−loop RNAs used in SPR measurements were biotinylated at the 5′ end (Dharmacon, Inc.) followed by a spacer sequence (CUCCC) to allow for optimal binding to the streptavidin chip. Stem−loop RNAs used in EMSAs and NMR experiments lacked the biotinylated linker at the 5′ end and were 5′ end labeled using [γ-^{32}P]ATP. The SL_{28} and 65-mer (SL + HDE) H2A-614 RNA samples used for NMR were synthesized, deprotected, and purified via PAGE by Dharmacon, Inc. The RNA samples were taken up in 20 mM potassium phosphate buffer, 20 mM KCl, and 0.02 mM EDTA (pH 6.8). The RNA was folded by being heated at 95 °C for 2 min and snap-cooled on ice for 10 min to ensure the lowest-energy hairpin conformer. The formation of the stem−loop structure (instead of a duplex) using this approach was confirmed by NMR. All RNA samples used for NMR were in a 90% H_2O/10% D_2O mixture in a volume of 240 μL. The sample concentration for the 65-mer (SL + HDE) was 50 μM and for the SL_{28} RNAs was between 0.2 and 1 mM as noted.

EMSAs. Wild-type and mutant SLBPs were incubated with the 5′-^{32}P-end-labeled stem−loop probe for 10−20 min on ice in binding buffer [20 mM Tris (pH 7.9), 20% glycerol, 100 mM KCl, 0.2 mM EDTA, 0.5 mM DTT, and 0.1 mg/mL BSA]. The total reaction volume (10 μL) was analyzed on an 8% native polyacrylamide Tris-borate gel run in Tris-borate buffer at 150 V for 1−1.5 h. The gel was dried at 80 °C for 2 h and then exposed to film.

Mass Spectrometry. Baculovirus-expressed phosphorylated and dephosphorylated SLBPs were treated with a chloroform/water/methanol to remove trace amounts of detergent as previously described.[26] The samples were reconstituted with 40 μL of a 2% ACN/97.9% H_2O/0.1% formic acid mixture. Twenty microliters of the dissolved sample was desalted using either a C4 (for phosphorylated and dephosphorylated FL-dSLBP) or a C18 (for the dSLBP RBD) Ziptip (Millipore). Bound proteins were eluted with 10 μL of a 60% ACN/39.9% H_2O/0.1% formic acid mixture. The desalted samples were then loaded onto a metal-coated glass capillary tip for direct infusion into a Waters Qtof-Micro mass spectrometer. Calibration of the instrument was conducted over a wide mass range (200−2200 Da in positive ion mode) using a sodium iodide standard prior to infusion of the sample. Positive mode ESI was set with capillary, sample cone, and extraction voltages of 3 kV, 25 V, and 2 V, respectively. Scanning was set at 0.6 s per scan with an interscan time of 100 ms. The Analyzer and Tof Penning pressure were set to 4.07×10^{-9} and 5.17×10^{-7}, respectively. Data were collected and analyzed with MassLynx (version 4.0). Collected raw data were smoothed twice with a mean smoothing method consisting of a smoothing window of ±3 and then deconvoluted with the MaxEnt 1 algorithm in the appropriate mass range.

Measurement of Off Rates by Competition Experiments Analyzed by an EMSA. *Drosophila* SLBPs were incubated with the 5′-^{32}P-end-labeled stem−loop probe for 30 min on ice in binding buffer [20 mM Tris (pH 7.9), 20% glycerol, 100 mM KCl, 0.2 mM EDTA, 0.5 mM DTT, and 0.1 mg/mL BSA]. The total reaction volume was 100 μL, which included 5 nM [γ-^{32}P]ATP-labeled probe and 0.5 mM protein. At the 0 min time point, 10 μL of the reaction mixture was removed and frozen at −80 °C as the reference, and the dissociation reaction was initiated by the addition of a 100-fold excess of cold unlabeled stem−loop RNA. The reaction mixture was kept at 37 °C, and 10 μL aliquots were removed at varying time points over a period of 2.5 days and kept at −80 °C. Time points were analyzed on an 8% native gel and then exposed to a PhosphorImager.

SPR. Kinetic SPR studies were performed on a BIAcore T100 (Biacore, Inc., Piscataway, NJ) instrument. Biotinylated

RNAs were chemically synthesized (Dharmacon Research, Boulder, CO) with a 5′ biotin tag, and the hairpins were prepared by being heated to 95 °C for 5 min and then snap cooled on ice. The RNAs were immobilized on BIAcore SA (streptavidin-coated) sensor chips. Prior to the coupling of the 5′ biotinylated RNA ligand onto the sensor chip, the chip was conditioned by three sequential injections (1 min each) of 1 M NaCl in 50 mM NaOH at a flow rate of 50 μL/min. A 1 μM solution of either the pre-mRNA or the RNA hairpin was used as a stock solution for immobilization onto the chip. The binding of RNA was monitored as the change in response units (RUs), and 60−70 RUs were captured on the sensor chip. No RNA ligand was coupled to the first and third channels that were maintained as reference flow cells. The chip was primed in BIAcore HBS-P buffer [10 mM Hepes (pH 7.4), 150 mM NaCl, and 0.005% Surfactant P20] until the drift in the baseline was no greater than ±5 RUs. The SLBP analyte concentrations were in the range of 2 nM to 18 μM, and all samples were prepared by dialyzing the SLBP stock solution against HBS-P buffer for 24 h.

For the determination of SLBP−RNA binding kinetics, SLBP was injected onto the chip in the "Kinetics" mode at a flow rate of 30 μL/min for 2 min followed by a 10 min dissociation phase during which only the HBS-P buffer was injected. All binding experiments were performed at 25 °C. The bound protein was removed by two 60 s injection bursts of regeneration buffer (3 M NaCl) to restore the baseline. Five sensorgrams were recorded with varying protein concentrations. The data were analyzed using BiaEvaluation T100 software. The control channel was subtracted; the sensorgrams were aligned, and the data were globally fit by least-squares analysis to a 1:1 Langmuir binding model. Both the association and dissociation phases were fit simultaneously. The best fit of the data was determined by the randomness of the residuals and the lowest χ^2 value obtained. Linear errors in the determination of k_{on} and k_{off} are reported from the best fits of the data, and standard error propagation methods were used for the determination of errors for K_a and K_d. At least two independent sets of measurements were performed for each protein.

Fluorescence Measurements. Fluorescence experiments were performed on a SPEX Fluorolog-3 spectrofluorometer at 25 °C. The association of SLBP with either stem−loop RNA or a nonspecific RNA that corresponded to a 30-nucleotide HDE sequence was monitored by following a decrease in the intrinsic tryptophan fluorescence ($\lambda_{excitation}$ = 295 nm; $\lambda_{emission}$ between 300 and 500 nm; $\lambda_{max,emission}$ = 385 nm) as a function of increasing RNA concentration. The concentration of SLBP was 5 μM, and the concentration of RNA varied from 5 to 200 μM. After the last titration point, the samples were stored at room temperature and the change in fluorescence intensity was monitored over a period of 6 days, which was determined to be the optimal time period for the reaction to reach equilibrium.

NMR Spectroscopy. One-dimensional (1D) ^{1}H NMR experiments for detection of RNA imino protons were conducted either on a Varian Inova 600 MHz spectrometer or on a Varian VNMRS 900 MHz spectrometer with a 5 mm cryogenic ^{1}H{^{13}C/^{15}N} probe. Each experiment was conducted with both a binomial 1−1 echo pulse with maximal excitation at 12.5 ppm for solvent suppression and an SS pulse for water suppression as a separate experiment. This was done to unambiguously determine whether intensity changes observed for the imino protons were real due to addition of the wild-type peptide or could be attributed to baseline distortions or the mode of water suppression. RNA samples were kept in 20 mM potassium phosphate buffer, 20 mM KCl, and 0.02 mM EDTA (pH 6.8). SLBP and peptides used for homonuclear NMR experiments were dissolved in 20 mM Tris acetate buffer, 50 mM NaCl, and a 90% H_2O/10% D_2O mixture. The pH or pD* of samples varied according to the experiment and is noted in the figure legends. 2D ^{1}H−^{1}H NOESY spectra were recorded on a 0.3 mM SL_{28} RNA, free and in the presence of a 6-fold excess of the 30-residue SLBP peptide at NMRFAM on the VNMRS 900 MHz spectrometer with a cryogenic probe. The NOESY data were collected with a mixing time of 125 ms at 1 °C with a binomial 1−1 echo pulse for solvent suppression. The exchangeable imino protons for the SL_{28}-UA RNA were assigned using 2D ^{1}H−^{1}H NOESY spectra (mixing times of 125 and 250 ms) collected in H_2O at 1 and 25 °C at 900 and 600 MHz. 2D NOESY spectra (125 and 250 ms) in D_2O at 25 °C and a 50 ms homonuclear 2D TOCSY spectrum at 600 MHz were also collected to assign the nonexchangeable protons of SL_{28}-UA RNA. One-dimensional ^{31}P NMR experiments were performed on a Varian Inova 500 MHz spectrometer using a broadband probe operating at a phosphorus frequency of 202 MHz. All ^{31}P NMR measurements were taken at 25 °C. For each experiment, 1000−20000 transients were collected with a 65° excitation pulse, a recycle delay of 3 s, and a sweep width of 98.7 ppm with proton decoupling. ^{31}P chemical shifts were referenced to 85% phosphoric acid. 2D ^{1}H−^{15}N HSQC spectra were recorded for uniformly ^{15}N-labeled dSLBP P231G at 900 MHz with a cryogenic probe at 25 °C and pH 6.0 in the presence and absence of RNA. The concentrations of the protein and the SL_{28}-UA RNA were 80 μM and 0.1 mM, respectively. ^{1}H−^{15}N HSQC spectra for the 30-mer and 20-mer peptides were collected at natural abundance on 40−50 mM samples (corresponding to a 0.15−0.2 mM uniformly ^{15}N isotopically labeled sample) in 20 mM Tris (pH 5), 50 mM NaCl, and 10% D_2O on an Inova 700 MHz spectrometer equipped with a cryoprobe at 283 K to decrease the solvent exchange of backbone amides. No evidence of aggregation was observed for the peptides under these conditions. The 30-mer and 20-mer peptides were assigned using standard 2D homonuclear NOESY (τ_m = 300 ms), TOCSY (isotropic mixing time using MLEV-17 of 100 ms), and DQF-COSY spectra acquired in States−TPPI mode with a 2 s steady state relaxation delay on 3−7 mM samples, 32−64 scans per t_1, with a matrix size of 1024 complex points in t_2 and 512−600 points in t_1, using WATERGATE for water suppression. NMR data were processed using a square-shifted sine bell (72−90°) and analyzed using Felix (Felix NMR) or NMRPipe. The tautomeric states of the histidines in the $WT_{20\text{-mer}}$ peptide were determined from a ^{1}H−^{15}N HMQC J experiment that used a 22 ms ^{1}H−^{15}N evolution period to refocus magnetization arising from the $^1J_{NH}$ couplings and to ensure that direct ^{1}H−^{15}N couplings were minimized.[27] The ^{15}N carrier was set to 205 ppm. For structure calculations, interproton distance restraints were obtained from 2D NOESY spectra (τ_m values of 80, 110, and 250 ms) acquired at 700 MHz on a 7 mM sample of the 30-mer peptide at 5 °C and dihedral angle restraints obtained from $^3J_{NH\alpha}$ couplings obtained from a high-resolution 2D DQF-COSY spectrum collected at 700 MHz. Structure calculations were performed using torsional dynamics simulations with CYANA 2.1 using standard simulated annealing protocols. NOE-based restraints were obtained from the CYANA automated NOE assignment protocol.

RESULTS

Secondary Structure in the Mouse Histone H2A-614 Pre-mRNA 3′UTR. Several mutagenesis studies have previously shown that the histone stem−loop mRNA has all the sequence determinants for specific and high-affinity recognition by SLBP.[20,28] However, SLBP plays an active role in stimulating histone pre-mRNA processing, particularly in histone genes that have a weaker HDE that cannot efficiently base pair with the U7 snRNP,[15] by either inducing structural rearrangements in the 3′UTR that facilitate U7 snRNP binding or promoting protein−protein interactions in the processing complex. Early on, Steitz and co-workers showed that proper processing of the histone mRNA requires a fixed distance between the stem−loop structure and the HDE.[29,30] One explanation for this molecular ruler hypothesis for precise cleavage after the stem−loop structure and the role of SLBP is that there may be other secondary structure elements in the 3′UTR that dictate processing. Recent biochemical experiments using enzymatic and chemical footprinting[31] suggest that the histone 3′UTRs of H4-12, H1t, and H2A-614 genes are structured such that the HDE sequence lies either in a second RNA hairpin or in a duplex and SLBP binding induces structural rearrangements in the 3′UTR. NMR studies[6] show that in the context of a 28-nucleotide stem−loop structure, the 5′ and 3′ flanking nucleotides are unstructured and have long ^{13}C relaxation times indicating that it is unlikely that the stem−loop structure is part of a pseudoknot.[6]

To determine whether the 3′UTR has other secondary structural elements besides the stem−loop motif, we collected 1D imino proton NMR spectra for a 65-nucleotide H2A-614 RNA that has both the stem−loop structure and the purine-rich HDE sequence and compared it to that of the 28-nucleotide stem−loop structure that has previously been characterized by NMR spectroscopy.[6] Computational predictions using UNA-Fold[32] suggest two possible structures may exist for this region (Figure 1A2,A3). The 1D imino proton NMR spectrum (Figure 1B) of the stem−loop RNA SL_{28}-UA (Figure 1 A1) shows five strong resonances in the Watson−Crick (W−C) base-paired region (12−15 ppm) corresponding to the stem of the hairpin as well as a weak U6 NH resonance for the closing U6-A11 base pair at 13.8 ppm (Figure 1A1,C), indicating that the imino proton of U6 is more prone to rapid exchange with bulk solvent. Intriguingly, at 25 °C, the spectrum of the 65-nucleotide SL + HDE RNA is almost identical to that of SL_{28}-UA with only one additional resonance at 12.5 ppm (Figure 1B), which, on the basis of the chemical shift, is likely to be a G-C base pair. However, when we performed a temperature titration and lowered the temperature to 5 °C (Figure 1C), at least three additional resonances appear in the W−C base-paired region of the SL + HDE RNA spectrum. Therefore, at least six additional nucleotides are capable of being base-paired in the absence of bound proteins or U7 snRNA, although the pairs may be solvent-exposed or be less stable than the stem−loop structure. These additional resonances do not appear in the spectrum of the SL_{28}-UA RNA at low temperatures (Figure 1C). Titration of a 20-fold molar excess of Mg^{2+} into the SL + HDE RNA sample did not result in the appearance of new resonances or cause spectral perturbations in the 1D imino spectra, indicating that Mg^{2+} did not induce structure in this region of the RNA. We conclude that the 65-nucleotide SL + HDE H2A-614 mRNA has residual structure that extends beyond the stem−loop motif, but the stem−loop sequence is the only stable element of secondary structure. It is not clear whether histone mRNA specific processing factors could stabilize the nascent structure in the downstream sequence of the pre-mRNA, and this is an avenue for future studies.

Structure of the SLBP RBD and Recognition of the Histone mRNA. Until now, the 105-amino acid SLBP RPD has been refractory to detailed structure calculation by NMR or crystallography. Computational approaches using secondary structure prediction algorithms and ab initio modeling suggest that the SLBP RPD has an all-helical RNA binding domain with either three or four helices (Figure 2A). This is consistent with the helical nature of the RPD previously characterized by NMR and circular dichroism.[19] All the SLBP RPD constructs we previously tested were not stably folded in solution. However, a peptide that corresponds to the first 30 residues of the human SLBP RPD (residues Glu129−Val158) and has many of the sequence determinants for RNA binding[18] was amenable to structure calculation by NMR. The solution NMR structure of residues Glu129−Val158 shows that this region folds into two helices separated by a short loop in solution (Figure 2C,D and Figure 2 of the Supporting Information). Helix 1 extends from Glu132 to Ile142 and helix 2 from Thr147 to Val158. Residues Arg137, Lys140, Tyr144, Asn147, Tyr151, and Tyr154 lie on one face of helix 1 forming an extensive basic and hydrophobic interface that likely contacts the RNA (Figure 2D). Residues important for RNA processing (Asp152, Arg153, Ile155, and Lys156)[18] are oriented on the opposing face in helix 2. The structure statistics are summarized in Table 1.

To determine whether this 30-residue peptide could form a complex with stem−loop histone mRNA, we performed SPR studies in which biotinylated stem−loop RNA was loaded onto a streptavidin sensor chip and the change in response was measured in the presence of increasing concentrations of HTH peptide (Figure 1D of the Supporting Information). However, no measurable interaction was observed between the HTH peptide and the stem−loop RNA. This result was confirmed by gel retardation experiments (data not shown). The K_D of the histone mRNA hairpin for this peptide is therefore greater than the upper limit for SPR (10^{-4} M). We concluded that either the helices are not oriented favorably for RNA recognition when removed from the context of the intact domain or formation of a stable and specific SLBP−RNA complex requires a second binding site C-terminal to the 30-residue RPD peptide.

NMR is uniquely suited for testing molecular interactions over a wide range of affinities. Therefore, we titrated the wild-type SLBP HTH peptide into different histone stem−loop RNAs and monitored spectral changes in the 1D imino proton NMR spectra in response to increasing concentrations of added peptide (Figure 3A,C). The titration was performed with a 1−1 echo or an SS pulse for water suppression to rule out artifactual changes due to the mode of solvent suppression or baseline correction. When the 30-residue peptide is titrated into either SL_{28}-CG or SL_{28}-UA (Figure 3), the only spectral change observed in the 1D imino ^1H spectrum is an increase in the intensity of the imino protons of the loop uridines (U7, U8, and U9) that lie in the unpaired region of the spectrum. These resonances are very broad at pH 6.8 and 25 °C but become more protected from exchange in the presence of the peptide. To determine whether these changes were due to small differences in the phosphate buffer of the titrated solution, we repeated a similar titration with phosphate buffer alone and did not observe any change in the intensity of the unpaired uridines (Figure 3C). We also titrated the 30-residue peptide into a

Table 1. NMR Structure Statistics for the SLBP RPD HTH Peptide

NMR distance and dihedral constraints	
distance constraints	
total NOE	409
intraresidue	166
inter-residue	243
sequential ($\|i - j\| = 1$)	145
medium-range ($\|i - j\| < 4$)	77
long-range ($\|i - j\| > 5$)	21
hydrogen bond	0
total dihedral angle restraints	
ϕ	18
structure statistics	
Ramachandran analysis (%)	
residues in most favored regions	86.1
residues in additional allowed regions	13.9
deviations from idealized geometry	
bond lengths (Å)	0.0048 ± 0.0002
bond angles (deg)	0.582 ± 0.017
average pairwise root-mean-square deviation, 20 conformers (Å)	
heavy atoms	1.72 ± 0.21
backbone atoms	0.90 ± 0.27

mutant form of the stem−loop motif, LSL_{28}, in which the loop uridines at positions 7 and 9 (Figure 3C) were replaced with adenosines. Titration of the peptide into the LSL_{28} RNA mutant resulted in a small increase in the intensity of the U8 resonance, but no other perturbation in the 1D imino proton spectrum was observed. Finally, to determine whether the effects were due to the nonspecific interaction of a basic peptide with the RNA, we titrated a mutant 30-mer peptide in which key arginines and tyrosines were replaced with lysines and alanines, respectively. This peptide was not expected to bind the RNA, and no changes in the 1D imino spectrum were observed (Figure 3B).

We also compared 2D NOESY data for SL_{28}-UA in the absence and presence of a 6-fold molar excess of the 30-mer peptide (Figure 4). 2D NOESY spectra were used to assign the imino protons of the stem. For the free SL_{28}-UA, five imino protons show clear sequential NH−NH NOEs in the W−C base pair region, whereas the U6 NH resonance is broad and observed only at 5 °C. Notably, a strong NOE is observed between the G1 NH and G2 NH resonances in the free RNA that lie at the base of the stem. However, addition of the peptide results in the loss of this sequential G1 NH−G2 NH NOE (Figure 4A). The cross-strand NOE from the G1 imino

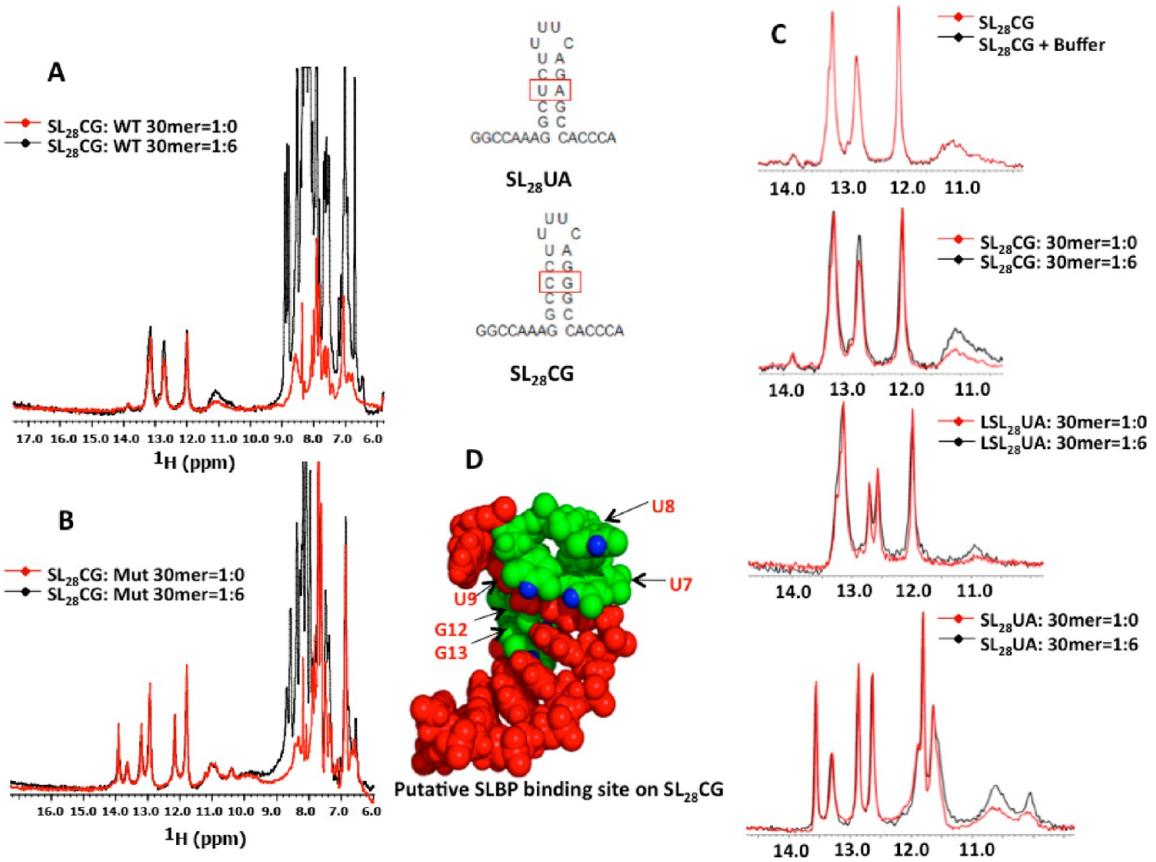

Figure 3. Interaction of the SLBP HTH motif with the histone mRNA hairpin monitored by 1D imino proton NMR spectra. (A) 1D ^{1}H imino NMR spectra (17−6.0 ppm) of the stem−loop RNA SL_{28}-CG in the presence of increasing concentrations of the HTH peptide collected at 1 °C and 600 MHz. The SL28 RNA:SLBP HTH peptide molar ratio is 1:6. The samples were in phosphate buffer (pH 6.8) as described in Materials and Methods. (B) 1D ^{1}H imino NMR spectra of the stem−loop RNA SL_{28}-UA in the presence of increasing concentrations of the mutant HTH peptide (see Materials and Methods) collected at 1 °C and 600 MHz. The SL28 RNA:SLBP HTH peptide molar ratio is 1:5. The increased level of protection of unpaired imino protons is not due to baseline corrections. (C) Imino region of the various 1D spectra superimposed to highlight the small increase in intensity of the unpaired uridine imino groups observed in the presence of the WT 30-mer peptide. No spectral change is observed with the buffer control. Both SL_{28}-CG and SL_{28}-UA show this effect. (D) U7, U8, and U9 uridine bases are colored green, and the imino protons that show protection from exchange in the presence of the HTH peptide are colored blue. Small but significant changes in peak intensities were also observed for G12 and G13.

dx.doi.org/10.1021/bi2018255 | *Biochemistry* 2012, 51, 3215−3231

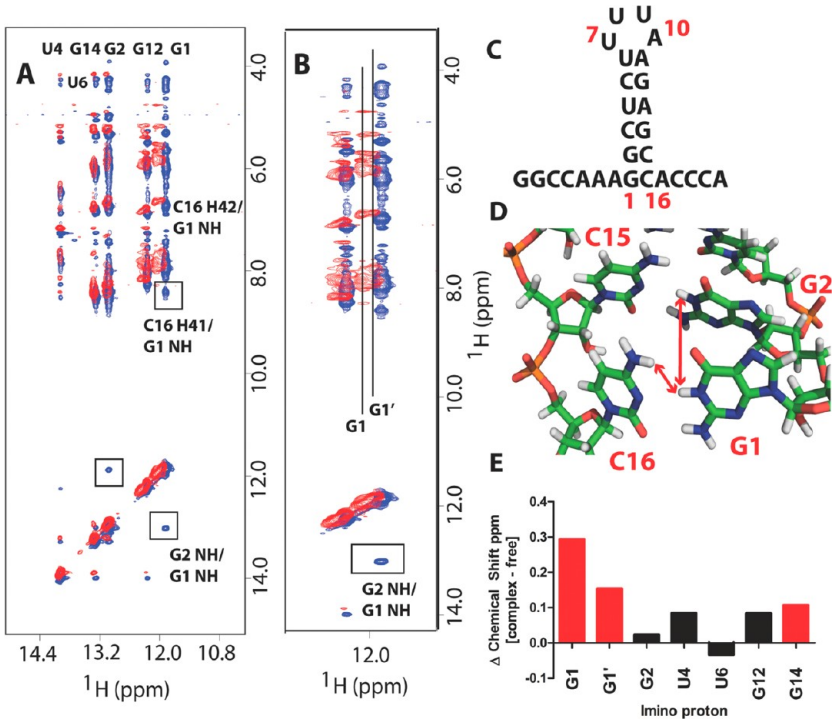

Figure 4. First G-C base pair at the base of the stem that is destabilized in the presence of the HTH peptide. (A) 2D ^{1}H−^{1}H NOESY data (125 ms) were collected at 900 MHz with cryoprobe on a 0.3 mM sample of SL28-UA at 1 °C as described in Materials and Methods. The imino region of the free RNA is colored blue, and the same region in the presence of a 6-fold excess of the HTH peptide is colored red. The most significant differences in the two spectra were the loss of the sequential G1−G2 imino−imino NOE that is characteristic of stem regions of RNA structure and the loss of the cross-strand NOE between the G1 NH and the C16 H4 amino proton. These NOEs are depicted on the structure of the SL28 RNA in panel D. In panel B, the expanded region of the NOESY spectrum is shown. In the presence of the HTH peptide, two unique conformations for the G1 NH are observed (highlighted and labeled G1 and G1′), both with a difference in chemical shift compared to that of the single conformation observed in free RNA. The secondary structure and numbering of the stem−loop RNA used are given in panel C. The difference in ^{1}H chemical shift for the imino protons between the RNA complexed to the 30-mer peptide and the free RNA is shown. Red bars show data for the imino protons for which the largest changes in chemical shift were observed. G1 and G1′ represent the two different conformations of the first guanine base at the bottom of the stem.

to the C16 H41 amino proton was also not observed in the presence of the peptide. The loss of these NOEs suggests that the first GC base pair is either destabilized or more exposed to solvent in the presence of peptide. Further evidence of the destabilization of the first base pair comes from the observation that two sets of resonances are found for G1 NH in the presence of the peptide (G1 and G1′), both of which are shifted by 0.24 and 0.11 ppm downfield compared to the single resonance observed for the G1 NH in the free RNA (Figure 4E). We also monitored NOE changes in the peptide in response to the addition of histone mRNA (Figures 2 and 7 of the Supporting Information). A number of peptide resonances were shifted or exchange-broadened in the presence of RNA. The broadening of the peptide resonances prevents detailed characterization of the peptide in the complex by NMR. Notably, chemical shift perturbations are observed for all three Tyr Hδ and Hε ring protons of the HTH (Figure 2 of the Supporting Information). Two tyrosines (Tyr151 and Tyr154) have previously been shown to be important for RNA recognition.[18] On the basis of the spectral changes observed in 1D and 2D NMR spectra, the data are consistent with the U7, U8, and U9 uridines in the RNA tetraloop possibly participating in stacking interactions with Tyr151 and Tyr154 in the SLBP HTH motif. We have shown that interaction of the SLBP peptide with the SL28 RNA destabilizes the first GC base pair in the stem.

Evidence of a second binding site C-terminal to the HTH peptide comes from fluorescence experiments. The interaction of baculovirus-expressed SLBP RPD with histone mRNA was followed by monitoring tryptophan fluorescence quenching as a function of RNA concentration (Figure 5). When histone stem−loop mRNA (SL_{28}) is added to a solution of phosphorylated SLBP, the fluorescence data show slow biphasic kinetics (Figure 5A). Initially, a rapid decrease in fluorescence intensity is observed at a red-shifted λ_{max} of 385 nm followed by a slow time-dependent and concentration-independent quench phase resulting in a 25% decrease in fluorescence intensity at 385 nm over the course of 5 days and an increase in fluorescence intensity at 442 nm (Figure 5B). The increase in fluorescence intensity at 442 nm results from FRET due to the transfer of electrons from the indole ring of one or more tryptophans in the C-terminus of the SLBP RPD to a purine or pyrimidine base in the RNA. This emission λ_{max} is close to that reported for cytidine (λ_{max} = 450 nm) upon excitation of tryptophan at pH 7 and 77 K.[33] The second and third base pairs (G-C and C-G) from the base of the histone mRNA stem are important for RNA binding, and it is likely that one or both cytosines make direct contacts via stacking interactions with one or more tryptophans in the C-terminus of the SLBP RPD. The time-dependent and concentration-independent change in fluorescence during the slow phase is not observed in the presence of a noncognate 30-nucleotide RNA sequence such as the histone downstream element (HDE30) (Figure 5C) or when dephosphorylated SLBP is incubated with the stem−loop RNA (Figure 5D). Therefore, there is a slow step in the reaction

dx.doi.org/10.1021/bi2018255 | Biochemistry 2012, 51, 3215−3231

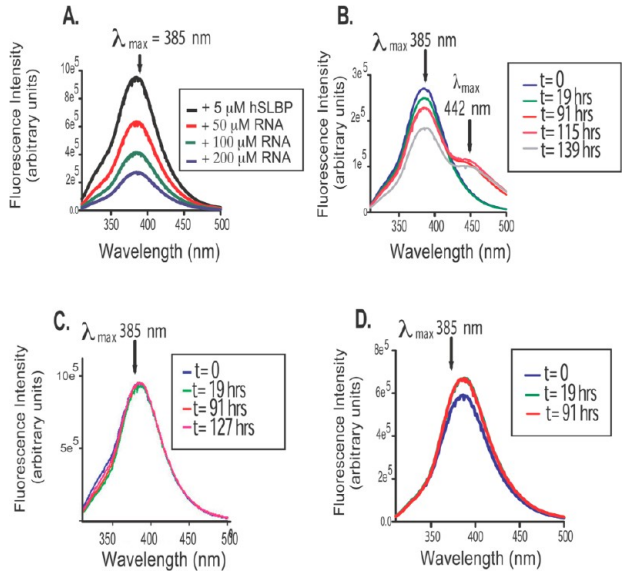

Figure 5. Second binding site for histone stem–loop RNA that exists C-terminal to the HPKTPNK sequence. Fluorescence emission spectra obtained after fluorescence excitation of intrinsic tryptophans at 295 nm. (A) Fluorescence quenching observed as a function of the increasing concentration of histone stem–loop RNA added. (B) Time-dependent fluorescence quenching observed with 5 μM hSLBP in the presence of 200 μM stem–loop RNA at 385 nm and a corresponding increase in fluorescence intensity observed at 442 nm resulting from Trp–cytosine FRET. (C and D) No time-dependent change in fluorescence is observed for (C) 5 μM hSLBP RPD in the presence of 200 μM HDE30 RNA or (D) 5 μM dephosphorylated SLBP RPD in the presence of histone stem–loop RNA.

mechanism for phosphorylated SLBP that reaches equilibrium over the course of days. As shown below, the SLBP RPD undergoes prolyl isomerization, the time scale of which ranges between 10 and 1000 s^{-1} due to a large energy barrier of 15–20 kcal/mol.[34] The slow equilibration phase of the phosphorylated SLBP–RNA complex is a direct consequence of proline isomerization in the absence of a peptidyl-prolyl isomerase.

Effect of Threonine Phosphorylation at Thr171 and Thr230 on the Kinetics of RNA Recognition. When phosphorylated at Thr171, which lies C-terminal to the HTH motif, human and *Xenopus* SLBPs have been reported to form very stable and specific complexes with the histone stem–loop structure.[20] Using nitrocellulose filter binding experiments, we previously showed that dephosphorylated SLBP exhibits a 6–8-fold lower affinity for histone mRNA.[22] Because filter binding experiments do not provide insight into the rates of RNA association and dissociation, we used surface plasmon resonance (SPR) to compare the on and off rates of phosphorylated and dephosphorylated full-length dSLBP and the minimal dSLBP RBD (residues 189–259) for the histone mRNA hairpin as well as the 65-nucleotide pre-mRNA (SL_{28} + HDE) we had characterized by NMR. When expressed in baculovirus, the full-length dSLBP is a heterogeneous mixture of multiple phosphorylated species but with only a single phosphorylation site in the RBD.[22] Consistent with this, the dSLBP RBD produced in baculovirus is a homogeneous protein that is phosphorylated only at Thr230 (Figure 6A). The phosphorylated RBD:dephosphorylated RBD ratio after purification is 100:2 as determined by mass spectrometry (Figure 6A). We attribute this high level of phosphorylation not to the unknown kinase that carries out the reaction in the cell but rather to the instability of the dephosphorylated form when overexpressed in either baculovirus or bacteria (M. Zhang and R. Thapar, unpublished observations). We were able to completely dephosphorylate the full-length dSLBP and dSLBP RBD proteins by incubating them with calf intestinal phosphatase for 12 h at 37 °C. Complete dephosphorylation was determined by a mobility shift on SDS–PAGE (Figure 6B) as well as a difference in the relative mobilities of the phosphorylated and dephosphorylated proteins in EMSAs (Figure 6C).

We used the phosphorylated and dephosphorylated full-length and RBD proteins to measure their respective interactions with the histone mRNA stem–loop structure and the pre-mRNA we have characterized in this study. The SPR-derived binding constants (Figure 6 and Figure 5 and Table 2 of the Supporting Information) reveal that the baculovirus-expressed phosphorylated full-length SLBP has a slow association rate for the histone mRNA stem–loop structure (k_{on} = 1.2 × 10^4 M^{-1} s^{-1}) compared to the diffusion-limited rate of 1.0 × 10^9 M^{-1} s^{-1} and a slow dissociation rate (k_{off} = 5.7 × 10^{-4} min^{-1}) yielding a binding constant (K_D) of 47.5 ± 17 nM (Table 2). Our K_D values reported by SPR measurements are higher than those previously reported by filter binding (K_D ~ 0.8–1.5 nM)[20] and could reflect possible differences in solution conditions, data fitting, and the methods used.

The first observation from the SPR studies is that the phosphorylated full-length dSLBP binds more favorably to the pre-mRNA such that the K_D increased by ~15-fold, corresponding to a $\Delta\Delta G$ of −1.6 kcal/mol. The dephosphorylated full-length dSLBP also had a higher affinity for the pre-mRNA [K_D(rel) = 5.6; $\Delta\Delta G$ = −1.0 kcal/mol]. The increased affinity for the pre-mRNA (defined here as the SL28 + HDE sequence) suggests that either direct contacts are made by SLBP to regions outside the stem–loop structure in the 65-nucleotide RNA used or the secondary structure of the stem–loop structure is slightly different in the context of the 65-nucleotide sequence.

Second, the minimal dSLBP RBD (residues 189–259) is not as effective in its interaction with either the stem–loop structure or the pre-mRNA as compared to the full-length dSLBP. All K_D values obtained were 20–200-fold higher for the dSLBP RBD than for full-length dSLBP. The phosphorylated RBD also shows a much smaller difference in the level of relative binding to the stem–loop structure versus the pre-mRNA [K_D(rel) = 1.65; $\Delta\Delta G$ = −0.3 kcal/mol]. Because the longer dSLBP RPD (residues 189–276) does bind histone mRNA as effectively as the full-length protein,[22] we interpret this to mean that the additional C-terminal residues and/or phosphorylation of the four serines in the C-terminus of the dSLBP RPD (between residues 259 and 276)[25] stabilizes the entire domain or is involved in direct contacts with the RNA.

Next, we determined the effect of dephosphorylating SLBP at Thr230 on histone mRNA recognition. The more basic dephosphorylated full-length SLBP has a 10-fold faster on rate toward the stem–loop structure but also a 100-fold faster off rate of 7.44 × 10^{-2} M^{-1} s^{-1}, yielding a K_D of 528.6 ± 73 nM. This corresponds to an ~11-fold decrease in binding affinity for dephosphorylated full-length dSLBP, which is very similar to what we previously reported using filter binding measurements.[22] An ~30-fold difference in affinity is observed for the phosphorylated and dephosphorylated dSLBPs toward the pre-mRNA sequence. We were not able to measure any reliable values for the interaction of the dephosphorylated RBD with stem–loop RNA, and the sensorgrams were more

dx.doi.org/10.1021/bi2018255 | *Biochemistry* 2012, 51, 3215–3231

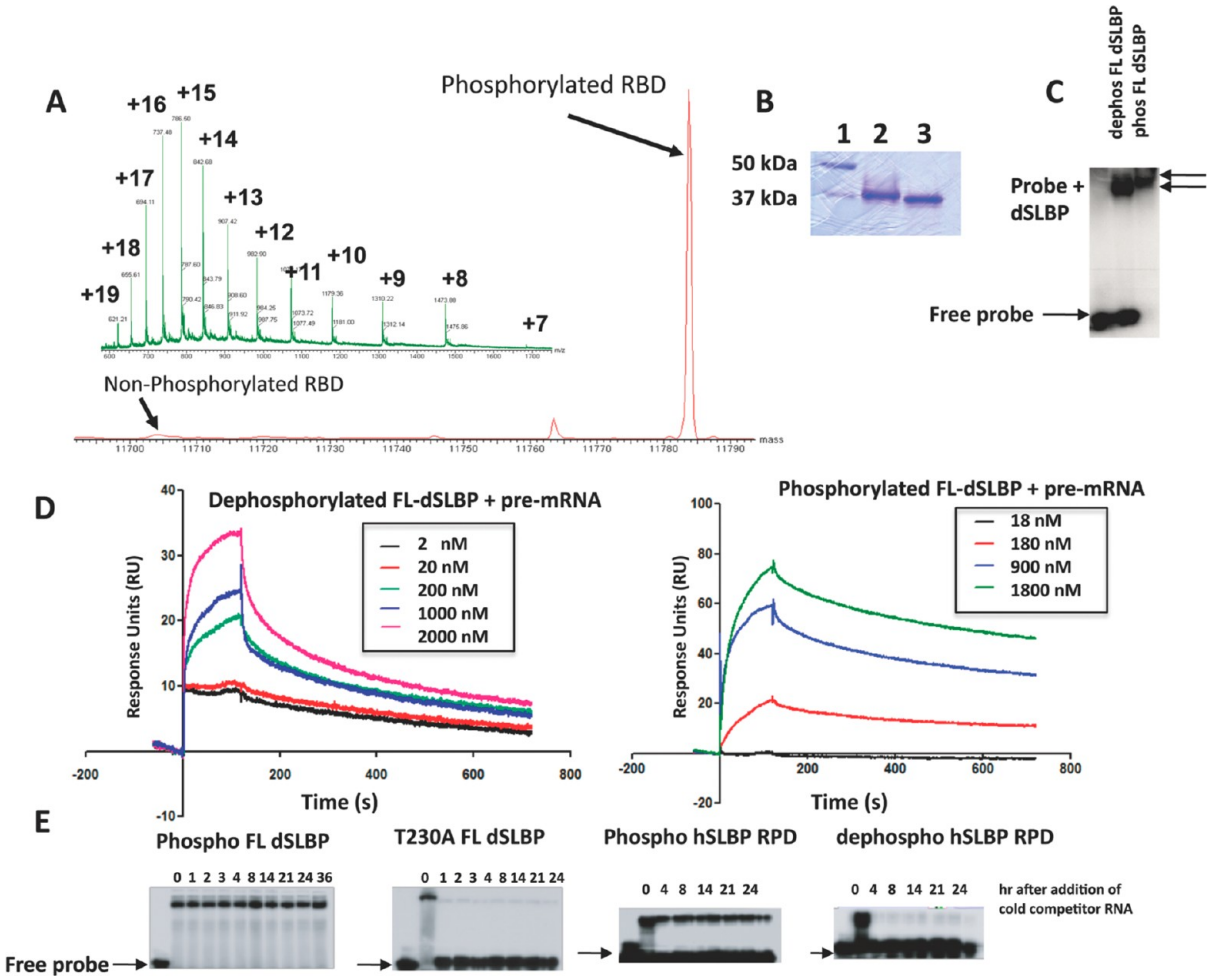

Figure 6. Effect of SLBP RPD phosphorylation on the kinetics of association with histone mRNA. (A) The electrospray mass spectrum (ES-MS) of the dSLBP RBD obtained on a Qtof-Micro mass analyzer is shown. The mass obtained was 11783.00 Da, corresponding to a single phosphate at Thr230, cleavage of the N-terminal Met, and acetylation of the N-terminal serine. On the basis of peak heights, the phosphorylated RBD:dephosphorylated RBD ratio was 100:2. (B) SDS−PAGE of full-length dSLBPs used for SPR. The molecular mass markers are in lane 1; the phosphorylated full-length dSLBP is in lane 2, and the dephosphorylated full-length dSLBP is in lane 3. (C) EMSA of the phosphorylated and dephosphorylated full-length dSLBPs shows a difference in mobility in a native gel. (D) Representative SPR sensograms for unphosphorylated and baculovirus-expressed phosphorylated *Drosophila* SLBP RPDs. The association phase was measured between 0 and 120 s and the dissociation phase up to 600 s. The baseline was re-established by regeneration of the chip with 3 M NaCl. (E) Dissociation of *Drosophila* SLBP full-length and human RPD proteins measured using an EMSA in the presence of a 100-fold excess of cold competitor RNA at 37 °C. All proteins were expressed in baculovirus. The hSLBP RPD was dephosphorylated where indicated by calf intestinal phosphatase.

Table 2. Rate Constants Derived from Surface Plasmon Resonance (SPR) for Full-Length *Drosophila* SLBP and the RBD (residues 189−259) toward Histone mRNA at 25 °C

	k_1 (M^{-1} s^{-1})	k_{-2} (s^{-1})	K_D (nM)	K_D(rel)[a]	$\Delta\Delta G$ (kcal/mol)
		Phosphorylated SLBP			
full-length dSLBP−SL28 RNA	1.2×10^4	5.7×10^{-4}	47.5 ± 17.0	14.8	1.6
full-length dSLBP−pre-mRNA	4.1×10^4	1.3×10^{-4}	3.2 ± 2.9	–	
RBD (residues 189−259)−SL28 RNA	6.9×10^3	8.7×10^{-2}	1268 ± 195	396.2	3.5
RBD (residues 189−259)−pre-mRNA	2119	1.63×10^{-3}	766.8 ± 138	239.6	3.2
		Dephosphorylated SLBP			
full-length dSLBP−SL28 RNA	1.4×10^5	7.4×10^{-2}	528.6 ± 73	165.2	3.0
full-length dSLBP−pre-mRNA	8522	8.05×10^{-4}	94.5 ± 18	29.5	2.0
RBD (residues 189−259)−SL28 RNA	unstable[b]	unstable[b]	unstable[b]	–	–
RBD (residues 189−259)−pre-mRNA	307.7	1.79×10^{-3}	5827 ± 115	1821	4.4

[a] K_D values relative to the interaction of full-length phosphorylated SLBP with the pre-mRNA sequence used. [b] See Figure 5 of the Supporting Information.

consistent with a heterogeneous analyte being present, indicating that truncation of the C-terminus and dephosphorylation of the RBD severely destabilize the protein (Figure 5 of the Supporting Information).

dx.doi.org/10.1021/bi2018255 | *Biochemistry* 2012, 51, 3215−3231

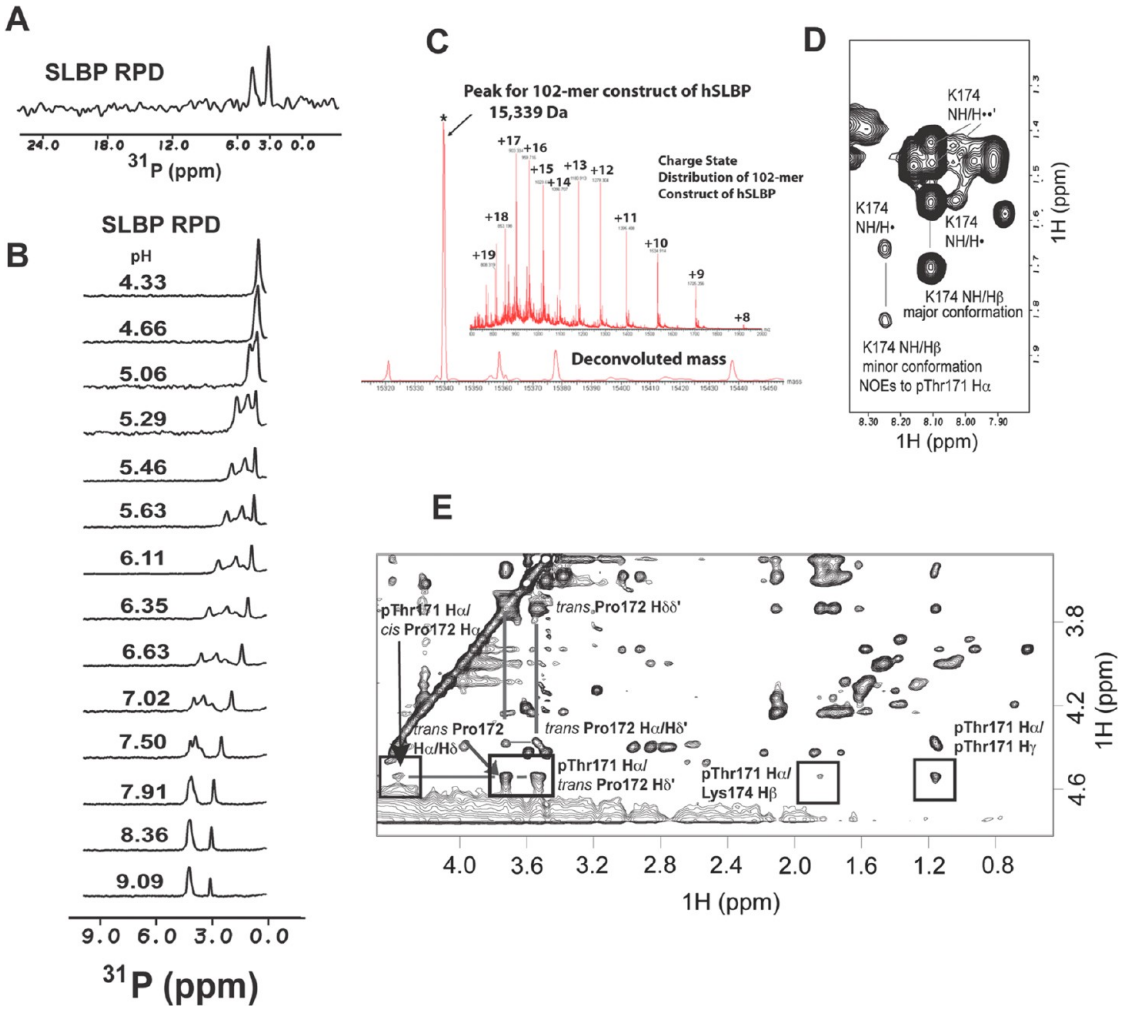

Figure 7. hSLBP RPD shows evidence for multiple conformations that are attributed to prolyl isomerization. (A) ^{31}P NMR spectrum of human SLBP RPD collected at 500 MHz, pH 8.1, and 25 °C. Two ^{31}P resonances are observed for the RPD that is phosphorylated only on a single threonine in the HPKTPNK sequence. (B) pH titration of the SLBP RPD monitored by ^{31}P NMR. (C) ESI-MS mass spectrum used for ^{31}P NMR of the SLBP RPD. The protein exists as a single species that is phosphorylated at only T171. (D) NH−aliphatic NOEs for the major and minor conformations of Lys174 are shown in the spectrum of the 20-mer unphosphorylated peptide, providing additional evidence that the peptides exist as two conformations that are in slow exchange on the NMR time scale. (E) Portion of the NOESY spectrum of the WT phosphopeptide (pepWT). The pattern of NOEs provides clear evidence of proline cis−trans isomerization about the phosphoThr171−Pro172 bond. The NOEs originating from the Hα chemical shift of phosphoThr171 are highlighted. As discussed in the text, a weak NOE is observed between the phosphoThr171 Hα atom and the Pro172 Hα atom that is diagnostic of a cis Pro conformation. Medium to strong NOEs are observed between the phosphoThr171 Hα atom and the Pro172 Hδ atom that are diagnostic of a trans Pro bond.

Measurements of on and off rates may also be performed using an EMSA or filter binding. Therefore, to test the validity of the SPR data, we measured the off rate in competition experiments using an EMSA (Figure 6E). In these experiments, a preformed SLBP−RNA complex was incubated with a 100-fold excess of cold competitor RNA at 37 °C and the dissociation of the radiolabeled RNA was monitored over the course of 24−36 h. As is clearly shown in Figure 6E, both phosphorylated full-length *Drosophila* SLBP and the phosphorylated human SLBP RPD have a slow off rate and the complex does not dissociate over 24 h. On the other hand, mutation of the threonine to alanine in *Drosophila* SLBP or dephosphorylation of baculovirus-expressed human SLBP RPD results in a complex in which the labeled RNA rapidly dissociates after the addition of cold competitor RNA. Therefore, the dephosphorylated form is characterized by rapid dissociation indicative of an unstable complex. Thus, phosphorylation at Thr171 is a key determinant in the formation of a stable complex.

The SLBP RPD Undergoes Prolyl Isomerization about the Thr171/230−Pro172/231 Peptide Bond. When expressed in baculovirus, the human SLBP RPD is also phosphorylated at only one site (Thr171), which was confirmed by mass spectrometry (Figure 7C). However, two ^{31}P NMR resonances are observed at pH 8.4 for the single phosphate (Figure 7A) at 3.00 and 4.19 ppm, both of which lie within the range of that expected for *O*-phosphothreonine (3−5 ppm). To determine the ionization state of the phosphoryl groups, the ^{31}P chemical shifts were followed as a function of pH and the response of this phosphate to a varying pH (4.33−9.09) was monitored by ^{31}P NMR (Figure 7B). Similar to inorganic phosphate (pK_a = 7.0 ± 0.01) and the *O*-phosphothreonine standard (pK_a = 6.3 ± 0.02), the ^{31}P resonances for the free protein go through a single ionization event corresponding to an apparent pK_a of 6.9. Therefore, in the absence of RNA, and at neutral pH, the phosphothreonine in free SLBP favors a dianionic form that is dominant in all the observed conformational

dx.doi.org/10.1021/bi2018255 | *Biochemistry* 2012, 51, 3215−3231

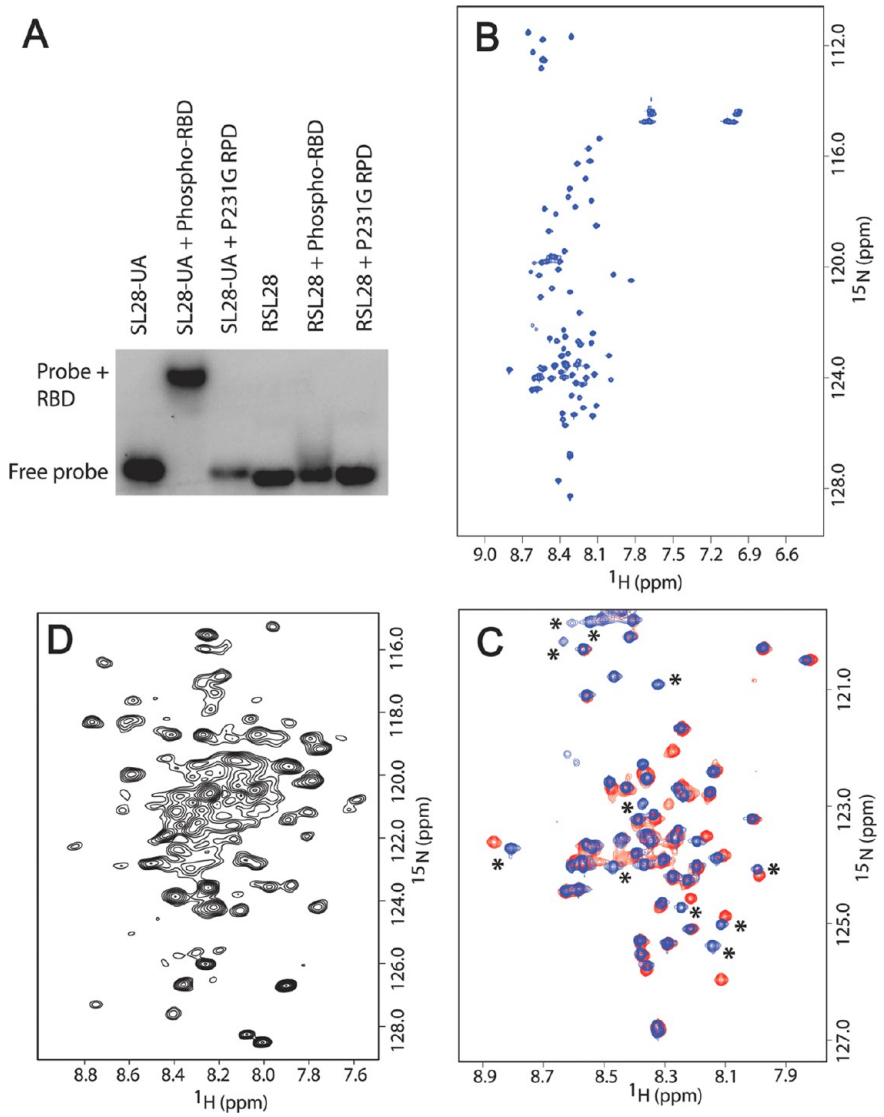

Figure 8. P231G dSLBP mutant that forms a single conformer that binds SL28 histone mRNA. (A) A 5′ ^{32}P-labeled SL_{28}-CG RNA was used to compare the affinity of the baculovirus-expressed phosphorylated dSLBP RBD to that of the bacterially expressed nonphosphorylated P231G mutant SLBP in EMSAs. The baculovirus-expressed dSLBP RBD forms a specific and high-affinity complex with SL_{28}-CG RNA but not with the RSL_{28}-CG mutant RNA. In contrast, the dSLBP P231G RBD does not shift the probe, but a decrease in the relative amount of free probe is observed, indicating that the complex likely dissociates throughout the gel due to weak binding. No binding was observed for the RSL_{28}-CG mutant. (B) ^{1}H−^{15}N HSQC spectrum of uniformly ^{15}N-labeled SLBP P231G RPD that shows a single conformation for all backbone amide resonances. The spectrum was collected on an 80 μM sample at 900 MHz with a cryoprobe at 25 °C. (C) Portion of the ^{1}H−^{15}N HSQC spectrum of the uniformly ^{15}N-labeled SLBP P231G RPD collected in the absence (blue) and presence (red) of an equimolar amount of unlabeled SL_{28}-CG RNA. (D) Portion of the ^{1}H−^{15}N HSQC spectrum of the wild-type ^{15}N-labeled dSLBP RPD collected at 700 MHz with a cryoprobe at 25 °C for comparison.

states. In addition, the NMR line widths for the ^{31}P resonances (3−5 ppm) are very broad between pH 5.5 and 8.0, and a number of conformational substates are observed for the phosphates in the free protein at neutral pH (Figure 7B). This suggests that the ^{31}P resonance is influenced by interactions in its local environment in addition to deprotonation of the orthophosphate. It is also consistent with our previous observations[19] using NMR that the SLBP RPD is not stably folded in the absence of RNA and undergoes conformational exchange among multiple states at physiological pH. A likely explanation for the observed conformational heterogeneity could be the presence of two prolines near the phosphothreonine in the HPKTPNK sequence that are potentially capable of generating four cis and trans proline conformers. In addition, the deprotonation of the phosphate may be coupled to the protonation state of His168.

To further characterize the properties of this region, we synthesized 20-residue unphosphorylated and Thr171/Thr230-phosphorylated peptides. The ^{1}H−^{15}N HSQC spectrum of the unphosphorylated 20-residue peptide corresponding to the sequence that follows the HTH motif (residues His161−Arg180 of human SLBP) and comprises the site of phosphorylation shows two sets of cross-peaks for 16 of 18 (20 residues − 2 Pro) expected amide resonances (Figure 3 of the Supporting Information), indicating that the unphosphorylated peptide interconverts slowly between two distinct conformations on the NMR time scale. When the ^{1}H−^{15}N HSQC spectrum of the WT unphosphorylated peptide is compared to that of a peptide in which two of the prolines (Pro169 and Pro172) are replaced with alanines, only a single set of cross-peaks was observed for backbone NH and side chain NH_2 resonances, suggesting that the

dx.doi.org/10.1021/bi2018255 | *Biochemistry* 2012, 51, 3215−3231

observed conformational heterogeneity in the peptide is most likely due to proline isomerization in the HPKTPNK sequence.

The 20-residue peptides have three prolines, two of which are close to the phosphothreonine in the HPKTPNK sequence. Assuming that the N-terminal proline (Pro165) does not substantially contribute to the backbone dynamics of the region in the peptides, there are four possible conformational states (trans/trans, trans/cis, cis/trans, and cis/cis) for the backbone around the HPKTPNK sequence. To determine what the major and minor conformational states were, we assigned the proton NMR resonances of the 20-residue unphosphorylated and threonine-phosphorylated peptides that correspond to the region C-terminal to the site of threonine phosphorylation (residues H161−R180) and analyzed the 2D NOESY spectra (Figure 7D,E). Analysis of NOESY spectra of the phosphorylated peptide (Figure 7E) shows that the major conformation at pH 4 is the P169 trans/P172 trans conformer, and a minor fraction of the peptide adopts a P169 trans/P172 cis conformation. The major conformer shows NOEs between the phosphoThr171 Hα proton and the Pro172 Hδ1 and Hδ2 protons that are diagnostic of a Pro trans conformation. In addition, a weak NOE is observed between the phosphoThr171 Hα atom and the Pro172 Hα atom that is indicative of a cis Pro conformer (Figure 7E). On the basis of NOE intensities as well as peak intensities for the observed conformers in TOCSY spectra, the population of the cis Pro conformation in the peptides is expected to be ~15%. Therefore, the peptides provide unequivocal evidence that the sequence around the phosphorylated threonine samples a number of conformational states that are at least in part attributed to cis−trans isomerization of one or more prolines.

To address whether the observed conformational heterogeneity of the dSLBP RPD was due to isomerization about the Thr230−Pro231 bond, we mutated Pro231 to glycine (Figure 8). Our rationale was that introduction of a glycine at this position should result in increased backbone dynamics allowing greater sampling of conformational states that may be conducive to RNA binding. As shown in panels B and C of Figure 8, the ^{1}H−^{15}N HSQC spectrum of the P231G mutant of the dSLBP RPD shows a single conformation in solution as compared to the ^{1}H−^{15}N HSQC spectrum of the wild-type dSLBP RPD (Figure 8D). We used an NMR chemical shift perturbation assay to test whether the dSLBP P231G mutant binds histone mRNA. When unlabeled SL_{28}-CG RNA is titrated into a solution of uniformly ^{15}N-labeled P231G dSLBP RPD, the backbone amides of ~21 residues are significantly perturbed in ^{1}H−^{15}N HSQC spectra, indicating that these SLBP amide resonances experience a change in their chemical and electronic environment in the presence of RNA. In addition, the dSLBP P231G protein formed a stoichiometric complex with equimolar amounts of histone stem−loop RNA (Figure 8C). The complex is in the slow chemical exchange regime on the NMR time scale, which is suggestive of a high-affinity complex. No evidence of a second conformation is observed in our studies either with or without the histone stem−loop mRNA. However, the dSLBP P231G RPD does not bind the histone stem−loop RNA with high affinity in an EMSA (Figure 8A) as compared to the baculovirus-expressed phosphorylated RBD. Because EMSAs detect only complexes that are highly stable during electrophoresis, the assay underestimates binding affinities if the complex dissociates in the gel because of a faster off rate, or if the amount of protein used is even 10-fold lower than the K_D for the interaction.[35] The data are consistent with our observation that both phosphorylation and the correct proline conformer are key determinants of stability for the SLBP−histone mRNA complex.

We conclude that the SLBP RPD undergoes cis−trans proline isomerization about the Thr230−Pro231 bond and the backbone dynamics of this "hinge" region appears to be critical for histone mRNA recognition.

Contribution of His168 to the Observed Conformational Heterogeneity. His168/His227 is invariant in all SLBPs,[36] and His-Pro sequences are also known to act as chemical catalysts, influencing proline isomerization rates in standard peptides.[37] Mutation of H168 to phenylalanine has previously been shown to abrogate binding to histone stem−loop mRNA in EMSAs.[18] To determine whether H168/H227 affects the conformational dynamics of the region around the phosphothreonine, we measured the pK_a values of His168 and His161 in the 20-mer phosphopeptides by following the chemical shift of the ^{1}Hε signal as a function of pH (Figure 6 of the Supporting Information). The phosphorylated WT peptide shows a depressed pK_a of 5.6 for the side chain of His168, whereas His161 has a pK_a value of 6.4, in the range expected for a histidine. A depressed pK_a for a histidine usually results from either a H-bonding interaction or its proximity to a basic residue. Two lysines, Lys170 and Lys174, are present in this sequence, and either could act as a base. Next we determined the tautomeric states of the two histidines in the phosphopeptides at pH 6.5 and 25 °C. The observed chemical shifts and intensities of the Nε2−Hε2, Nε2−Hδ2, and Nδ1−Hε1 cross-peaks are in agreement with a neutral tautomeric state in which only His168 Nε1 is protonated. On the other hand, His161 exists in a charged state where both side chain nitrogens are protonated. To see whether replacement of His168 with Ala altered the ionization of the phosphoryl group, we performed ^{31}P titrations as a function of pH (Figure 9A−C). Two ^{31}P resonances are observed in the $WT_{20\text{-mer}}$ and $MUT_{20\text{-mer}}$ peptides as is observed in the context of the SLBP RPD, although the major conformer predominates. Replacement of His168 with Ala showed no change in either the relative populations of the major and minor components or the pK_a of ionization of the phosphate. It is conceivable that His168 may modulate the rates of cis−trans proline isomerization in the HPKTPNK sequence and thereby play an indirect role in RNA recognition. Alternatively, it may directly interact with histone mRNA. However, it does not appear to be a major contributor to the observed conformational heterogeneity of the SLBP RPD.

DISCUSSION

The data presented in this paper provide new insights into the mechanism of SLBP−histone mRNA recognition and the structural role of posttranslational modifications in RNA−protein interactions. We show that the SLBP RPD is α-helical and appears to recognize at least two distinct sites on the histone stem−loop structure using two distinct binding interfaces in its RPD (Figure 10). The first binding site on the SLBP RPD comprises residues Glu129−Val158 (human SLBP numbering), which forms a highly basic interface presented by helix 1 and loop 1. The second binding site on the hSLBP RPD appears to lie between Arg180 and Pro200 that is C-terminal to the site of threonine phosphorylation. Critical determinants in the RNA stem−loop structure for SLBP binding have previously been shown to be the second GC base pair in the stem, uridines 7 and 9 in the loop, and the

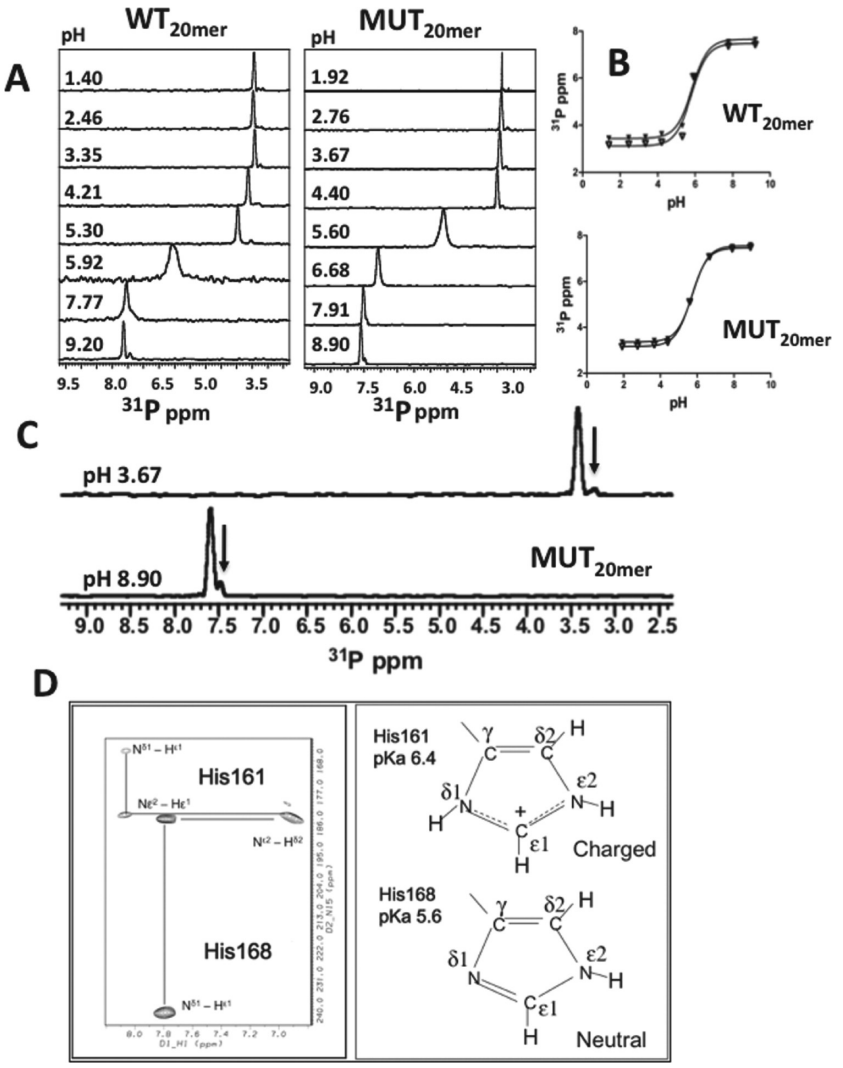

Figure 9. Role of His168 in the HPKTPNK sequence in the observed conformational heterogeneity of the SLBP RPD. (A) A 20-residue threonine-phosphorylated peptide corresponding to the WT sequence and a mutant 20-residue peptide in which His168 was replaced by alanine were used. The sequences of the peptides are given in Materials and Methods. The peptides were taken up in 20 mM Tris acetate buffer (pH 6.8), 50 mM NaCl, and a 90% H_2O/10% D_2O mixture. The dependence of the ^{31}P chemical shifts on pH was monitored. (B) Change in chemical shift plotted as a function of pH to obtain the pK_a for the ionization of the phosphate. Filled triangles represent data for the major conformer and empty triangles data for the minor conformer. (C) Expanded portion of the ^{31}P NMR spectra for the mutant peptide at two different pH values. Arrows point to the minor conformer in the peptide that was also observed in the WT peptide. (D) Portions of $^{1}H-^{15}N$ HMQC J spectra of the WT phosphopeptide (left) and tautomeric states of the histidines (right). The spectra were collected using phosphopeptides at natural abundance at 700 MHz using a cryoprobe at 25 °C and pH 6.5.

adenosines at positions −2 and 3 before the stem,[20] suggesting that there are multiple contacts between SLBP and the RNA target. The protection of loop uridine imino protons (U7, U8, and U9) from exchange with the solvent in the presence of the HTH peptide that we observed in this study is consistent with this region forming a binding interface for SLBP, possibly via stacking interactions with conserved tyrosines in the SLBP HTH motif. This interaction also destabilizes the first G-C base pair, "opening up" the base of the A-form stem. This may allow access of the SLBP RPD to the second GC base pair that is critical for sequence specific recognition of the RNA. In addition, the observation of FRET at 442 nm when the phosphorylated SLBP RPD is titrated into stem−loop RNA suggests that one or more of the conserved tryptophans toward the C-terminus of SLBP may be oriented toward the base of the RNA stem−loop structure and stack with either one or both G-C base pairs at the base of the stem−loop structure and/or with the adenosines 5′ of the stem−loop structure. Our data suggest that the HPKTPNK sequence is a critical hinge region. The role of phosphorylation and prolyl isomerization in SLBP may be to orient the C-terminus of the RPD toward the base of the RNA stem and the single-stranded flanking regions in an "active" conformation. The existence of two binding sites on SLBP for double-stranded and single-stranded RNA interacting regions indicates that a unique mode of RNA recognition is employed in contrast to other modular RNA binding domains and could explain how high affinity and specificity are achieved by SLBP (Figure 6). A more complete understanding of how SLBP contacts histone mRNA awaits NMR and X-ray crystallographic structures of the complex.

What are the possible roles of phosphorylation and prolyl isomerization of the SLBP RPD? From a functional perspective, threonine phosphorylation and prolyl isomerization of the SLBP RPD may allow the SLBP RNA binding domain to adopt

dx.doi.org/10.1021/bi2018255 | *Biochemistry* 2012, 51, 3215−3231

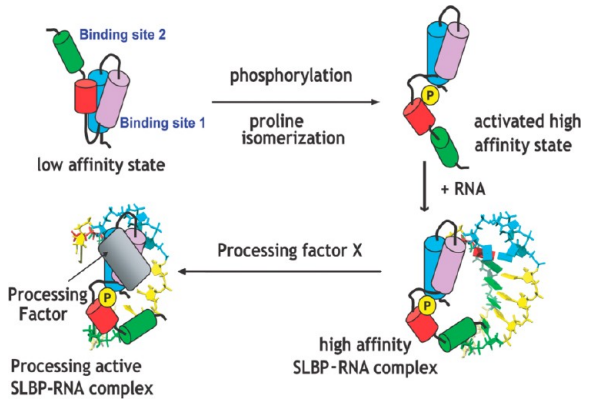

Figure 10. Our proposed model for how SLBP recognizes histone stem–loop mRNA and the role of phosphorylation and prolyl isomerization in RNA recognition. The SLBP RPD can exist in two unique conformational states of low and high activity, i.e., a major, low-affinity state and a scarcely populated, activated, high-affinity state. Phosphorylation populates the high-affinity conformation that is captured by the RNA. Once bound, SLBP forms a stable complex with the histone mRNA hairpin and may interact with another factor in the pre-mRNA processing reaction, thereby participating in 3′ end formation.

a unique structure that is recognized by another protein in the processing complex. Consistent with this, mutation of the threonine to alanine in *Drosophila* SLBP (T230A SLBP) results in misprocessing of the histone pre-mRNA in vitro and in vivo.[23] A full-length T230A mutant *Drosophila* SLBP (equivalent to T171A in human SLBP) is also unable to restore viability to *Drosophila* SLBP null mutants, indicating that phosphorylation at T230 is critical for the function of *Drosophila* SLBP in the cell. In unpublished studies from our laboratory (N. Krishnan and R. Thapar, manuscript in preparation), we find that the phosphorylated TPNK sequence in the SLBP RPD is a substrate for the prolyl isomerase Pin1 in vivo and in vitro. Pin1 regulates cis–trans prolyl isomerization about the Thr171–Pro172 bond, dissociating SLBP from the histone mRNA complex in vitro and regulating the SLBP ubiquitination and histone mRNA decay in vivo.

From a structural perspective, our studies highlight the importance of dynamics in RNA–protein interactions. We have shown in this study that phosphorylation at this conserved threonine is a key determinant for the stability of the SLBP–RNA complex and that the SLBP RPD exists in multiple folded conformations that are attributed to proline isomerization. Threonine phosphorylation occurs in a highly basic region of the RBD, and both positions N − 1 and N + 4 from the Thr are conserved Arg/Lys residues in all SLBPs. Therefore, it is likely that the interaction of the phosphate with Lys and Arg residues in its proximity stabilizes the domain. Phosphorylation may also alter the conformational equilibrium among multiple states, thereby affecting conformational capture by the RNA. In such a model, the RNA binding domain would interconvert among multiple conformations, only one of which binds RNA with high affinity. Quantitative studies of model peptides in the literature have shown that the introduction of a phosphate on a Ser/Thr N-terminal to a proline increases the cis Pro content in peptides by changing the thermodynamic equilibrium for prolyl bond isomerization.[38] In the absence of a PPIase, the cis–trans isomerization rate is 8-fold slower for a Thr/Ser-phosphorylated peptide than for an unphosphorylated peptide. Intriguingly, we observe a similar 6–15-fold stabilizing effect of phosphorylation on the affinity for the stem–loop RNA, by filter binding experiments as well as SPR. The P231G SLBP mutation may alter conformational sampling to favor the binding competent conformation in SLBP. Therefore, phosphorylation and prolyl isomerization of the SLBP RPD likely play both structural and regulatory roles in histone pre-mRNA processing and histone mRNA metabolism.

Finally, we provide NMR evidence that the SL + HDE region of the pre-mRNA has secondary structure beyond the stem–loop motif. An important question in the field of histone pre-mRNA processing is how the two cis elements, namely, the stem–loop structure and the HDE, cooperate to stimulate histone 3′ end formation. We suggest that the two essential cis elements, the stem–loop structure and the HDE, may be involved in a higher-order RNA structure that is necessary for specific recognition by the multifactor protein complex that catalyzes the cleavage reaction. Ongoing studies will test this hypothesis.

■ ASSOCIATED CONTENT

Ⓢ Supporting Information

Supplementary data, including seven figures. This material is available free of charge via the Internet at http://pubs.acs.org.

Accession Codes

The coordinates have been deposited in the Protein Data Bank (entry 2kjm) and the assignments for the 30-mer and 20-mer RPD peptides deposited in the BioMagResBank (entries 16274 and 16323, respectively).

■ AUTHOR INFORMATION

Corresponding Author

*Telephone: (716) 898-8687. Fax: (716) 898-8660. E-mail: rthapar@hwi.buffalo.edu.

Funding

These studies were supported by National Institutes of Health Grants 1RO1-GM076660 and 1RO1-GM076660-04S1 (ARRA) to W.F.M. and R.T. and faculty startup funds from the Hauptman-Woodward Medical Research Institute to R.T.

Notes

The authors declare no competing financial interest.

■ ACKNOWLEDGMENTS

The NMR studies were performed at the National Magnetic Resonance Facility at Madison (NMRFAM), the University of North Carolina Biomolecular NMR facility, and the University of Rochester School of Medicine and Dentistry. NMRFAM is supported by National Institutes of Health (NIH) Grants P41RR02301 (BRTP/NCRR) and P41GM66326 (NIGMS). Additional equipment was purchased with funds from the University of Wisconsin, the NIH (RR02781 and RR08438), the National Science Foundation (DMB-8415048, OIA-9977486, and BIR-9214394), and the U.S. Department of Agriculture. The biophysical experiments were performed at the Hauptman-Woodward Medical Research Institute and the Center of Excellence, SUNY at Buffalo. We sincerely thank Dr. Joseph P. Balthasar (School of Pharmacy, SUNY at Buffalo) for use of the SPR BIAcore T100. We also thank Dr. Scott Kennedy (University of Rochester, Rochester, NY) for advice with collection of NMR data on the RNA and for critical reading of the manuscript. We also appreciate Edward Z. Voss (W. M. Keck Foundation Biotechnology Resource Lab, Yale

University) for assistance with collecting some of the mass spectrometry data.

REFERENCES

(1) Marzluff, W. F., Wagner, E. J., and Duronio, R. J. (2008) Metabolism and regulation of canonical histone mRNAs: Life without a poly(A) tail. *Nat. Rev. Genet. 9*, 843−854.
(2) Li, G., and Reinberg, D. (2011) Chromatin higher-order structures and gene regulation. *Curr. Opin. Genet. Dev. 21*, 175−186.
(3) Gardner, K. E., Allis, C. D., and Strahl, B. D. (2011) OPERating ON Chromatin, a Colorful Language where Context Matters. *J. Mol. Biol. 409*, 36−46.
(4) Birchmeier, C., Folk, W., and Birnstiel, M. L. (1983) The terminal RNA stem-loop structure and 80 bp of spacer DNA are required for the formation of 3′ termini of sea urchin H2A mRNA. *Cell 35*, 433−440.
(5) Birnstiel, M. L., Busslinger, M., and Strub, K. (1985) Transcription termination and 3′ processing: The end is in site! *Cell 41*, 349−359.
(6) DeJong, E. S., Marzluff, W. F., and Nikonowicz, E. P. (2002) NMR structure and dynamics of the RNA-binding site for the histone mRNA stem-loop binding protein. *RNA 8*, 83−96.
(7) Zanier, K., Luyten, I., Crombie, C., Muller, B., Schumperli, D., Linge, J. P., Nilges, M., and Sattler, M. (2002) Structure of the histone mRNA hairpin required for cell cycle regulation of histone gene expression. *RNA 8*, 29−46.
(8) Wang, Z. F., Whitfield, M. L., Ingledue, T. C. III, Dominski, Z., and Marzluff, W. F. (1996) The protein that binds the 3′ end of histone mRNA: A novel RNA-binding protein required for histone pre-mRNA processing. *Genes Dev. 10*, 3028−3040.
(9) Martin, F., Schaller, A., Eglite, S., Schumperli, D., and Muller, B. (1997) The gene for histone RNA hairpin binding protein is located on human chromosome 4 and encodes a novel type of RNA binding protein. *EMBO J. 16*, 769−778.
(10) Dominski, Z., Erkmann, J. A., Yang, X., Sanchez, R., and Marzluff, W. F. (2002) A novel zinc finger protein is associated with U7 snRNP and interacts with the stem-loop binding protein in the histone pre-mRNP to stimulate 3′-end processing. *Genes Dev. 16*, 58−71.
(11) Yang, X. C., Burch, B. D., Yan, Y., Marzluff, W. F., and Dominski, Z. (2009) FLASH, a proapoptotic protein involved in activation of caspase-8, is essential for 3′ end processing of histone pre-mRNAs. *Mol. Cell 36*, 267−278.
(12) Kolev, N. G., and Steitz, J. A. (2005) Symplekin and multiple other polyadenylation factors participate in 3′-end maturation of histone mRNAs. *Genes Dev. 19*, 2583−2592.
(13) Dominski, Z., Yang, X. C., and Marzluff, W. F. (2005) The polyadenylation factor CPSF-73 is involved in histone−pre-mRNA processing. *Cell 123*, 37−48.
(14) Friend, K., Lovejoy, A. F., and Steitz, J. A. (2007) U2 snRNP binds intronless histone pre-mRNAs to facilitate U7-snRNP-dependent 3′ end formation. *Mol. Cell 28*, 240−252.
(15) Dominski, Z., Zheng, L. X., Sanchez, R., and Marzluff, W. F. (1999) Stem-loop binding protein facilitates 3′-end formation by stabilizing U7 snRNP binding to histone pre-mRNA. *Mol. Cell. Biol. 19*, 3561−3570.
(16) Sullivan, K. D., Mullen, T. E., Marzluff, W. F., and Wagner, E. J. (2009) Knockdown of SLBP results in nuclear retention of histone mRNA. *RNA 15*, 459−472.
(17) Sanchez, R., and Marzluff, W. F. (2002) The stem-loop binding protein is required for efficient translation of histone mRNA in vivo and in vitro. *Mol. Cell. Biol. 22*, 7093−7104.
(18) Dominski, Z., Erkmann, J. A., Greenland, J. A., and Marzluff, W. F. (2001) Mutations in the RNA binding domain of stem-loop binding protein define separable requirements for RNA binding and for histone pre-mRNA processing. *Mol. Cell. Biol. 21*, 2008−2017.
(19) Thapar, R., Marzluff, W. F., and Redinbo, M. R. (2004) Electrostatic contribution of serine phosphorylation to the *Drosophila* SLBP−histone mRNA complex. *Biochemistry 43*, 9401−9412.
(20) Battle, D. J., and Doudna, J. A. (2001) The stem-loop binding protein forms a highly stable and specific complex with the 3′ stem-loop of histone mRNAs. *RNA 7*, 123−132.
(21) Thapar, R., Mueller, G. A., and Marzluff, W. F. (2004) The N-terminal domain of the *Drosophila* histone mRNA binding protein, SLBP, is intrinsically disordered with nascent helical structure. *Biochemistry 43*, 9390−9400.
(22) Borchers, C. H., Thapar, R., Petrotchenko, E. V., Torres, M. P., Speir, J. P., Easterling, M., Dominski, Z., and Marzluff, W. F. (2006) Combined top-down and bottom-up proteomics identifies a phosphorylation site in stem-loop-binding proteins that contributes to high-affinity RNA binding. *Proc. Natl. Acad. Sci. U.S.A. 103*, 3094−3099.
(23) Lanzotti, D. J., Kupsco, J. M., Yang, X. C., Dominski, Z., Marzluff, W. F., and Duronio, R. J. (2004) *Drosophila* stem-loop binding protein intracellular localization is mediated by phosphorylation and is required for cell cycle-regulated histone mRNA expression. *Mol. Biol. Cell 15*, 1112−1123.
(24) Kodama, Y., Rothman, J. H., Sugimoto, A., and Yamamoto, M. (2002) The stem-loop binding protein CDL-1 is required for chromosome condensation, progression of cell death and morphogenesis in *Caenorhabditis elegans*. *Development 129*, 187−196.
(25) Dominski, Z., Yang, X. C., Raska, C. S., Santiago, C., Borchers, C. H., Duronio, R. J., and Marzluff, W. F. (2002) 3′ end processing of *Drosophila melanogaster* histone pre-mRNAs: Requirement for phosphorylated *Drosophila* stem-loop binding protein and coevolution of the histone pre-mRNA processing system. *Mol. Cell. Biol. 22*, 6648−6660.
(26) Wessel, D., and Flugge, U. I. (1984) A method for the quantitative recovery of protein in dilute solution in the presence of detergents and lipids. *Anal. Biochem. 138*, 141−143.
(27) Pelton, J. G., Torchia, D. A., Meadow, N. D., and Roseman, S. (1993) Tautomeric states of the active-site histidines of phosphorylated and unphosphorylated IIIGlc, a signal-transducing protein from *Escherichia coli*, using two-dimensional heteronuclear NMR techniques. *Protein Sci. 2*, 543−558.
(28) Williams, A. S., and Marzluff, W. F. (1995) The sequence of the stem and flanking sequences at the 3′ end of histone mRNA are critical determinants for the binding of the stem-loop binding protein. *Nucleic Acids Res. 23*, 654−662.
(29) Scharl, E. C., and Steitz, J. A. (1994) The site of 3′ end formation of histone messenger RNA is a fixed distance from the downstream element recognized by the U7 snRNP. *EMBO J. 13*, 2432−2440.
(30) Cho, D. C., Scharl, E. C., and Steitz, J. A. (1995) Decreasing the distance between the two conserved sequence elements of histone pre-messenger RNA interferes with 3′ processing in vitro. *RNA 1*, 905−914.
(31) Jaeger, S., Martin, F., Rudinger-Thirion, J., Giege, R., and Eriani, G. (2006) Binding of human SLBP on the 3′-UTR of histone precursor H4-12 mRNA induces structural rearrangements that enable U7 snRNA anchoring. *Nucleic Acids Res. 34*, 4987−4995.
(32) Markham, N. R., and Zuker, M. (2008) UNAFold: Software for nucleic acid folding and hybridization. *Methods Mol. Biol. 453*, 3−31.
(33) Helene, C., and Montenay-Garestier, T. (1968) Excitation energy transfer in molecular aggregates of nucleic acid derivatives in frozen aqueous solutions. *Chem. Phys. Lett. 2*, 25−28.
(34) Fischer, S., Michnick, S., and Karplus, M. (1993) A mechanism for rotamase catalysis by the FK506 binding protein (FKBP). *Biochemistry 32*, 13830−13837.
(35) Matos, R. G., Barbas, A., and Arraiano, C. M. (2010) Comparison of EMSA and SPR for the characterization of RNA-RNase II complexes. *Protein J. 29*, 394−397.
(36) Davila Lopez, M., and Samuelsson, T. (2008) Early evolution of histone mRNA 3′ end processing. *RNA 14*, 1−10.
(37) Davis, R. B. Jr., and Lecomte, J. T. (2006) A dynamic N-capping motif in cytochrome b5: Evidence for a pH-controlled conformational switch. *Proteins 63*, 336−348.

(38) Schutkowski, M., Bernhardt, A., Zhou, X. Z., Shen, M., Reimer, U., Rahfeld, J. U., Lu, K. P., and Fischer, G. (1998) Role of phosphorylation in determining the backbone dynamics of the serine/threonine-proline motif and Pin1 substrate recognition. *Biochemistry 37*, 5566−5575.